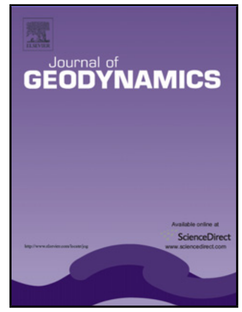

Title: Tectonic fabrics vs. mineralogical artifacts in AMS analysis: A case study of the Western Morocco extensional Triassic basins

Author: B. Oliva-Urcia A.M. Casas B. Moussaid J.J. Villalaín H. El Ouardi R. Soto S. Torres-López T. Román-Berdiel

PII: S0264-3707(16)30014-X
DOI: http://dx.doi.org/doi:10.1016/j.jog.2016.01.004
Reference: GEOD 1398

To appear in: *Journal of Geodynamics*

Received date: 13-8-2015
Revised date: 25-1-2016
Accepted date: 25-1-2016

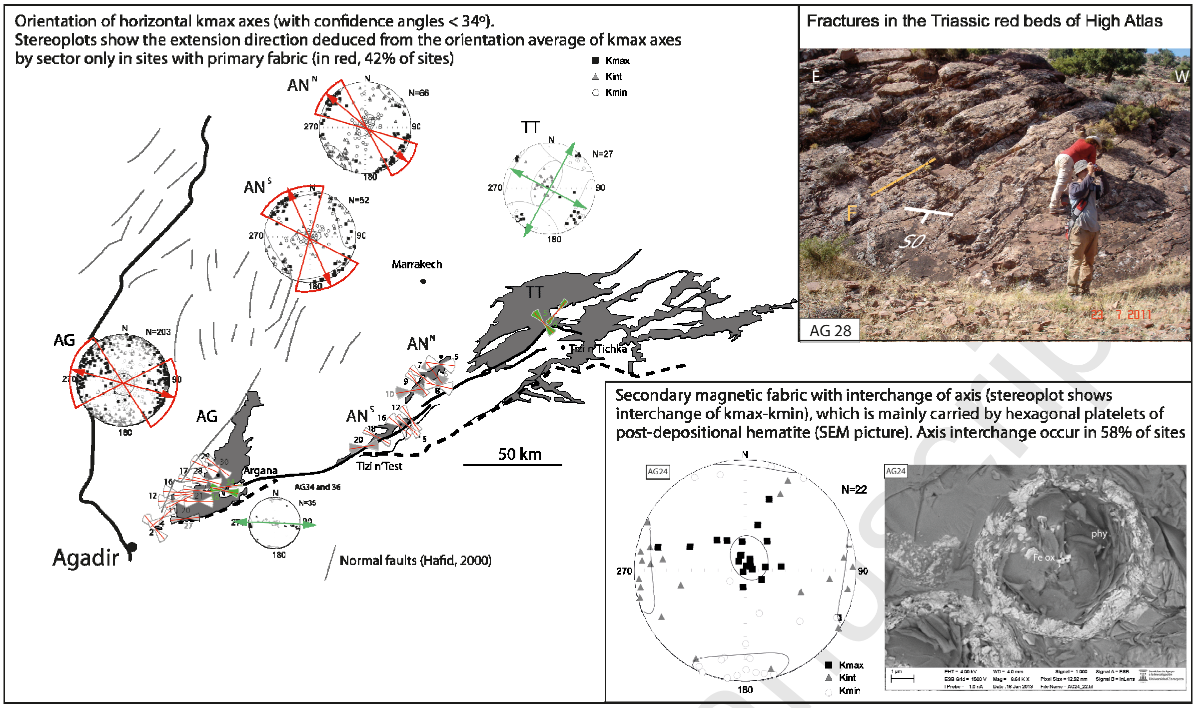

Graphical abstract

Tectonic fabrics vs. mineralogical artifacts in AMS analysis: A case study of the Western Morocco extensional Triassic basins

B. Oliva-Urcia[1,2], A.M. Casas[2], B. Moussaid[3], J.J. Villalaín[4], H. El Ouardi[5], R. Soto[6], S. Torres-López[4], T. Román-Berdiel[2]

1. Dpto. de Geología y Geoquímica. Universidad Autónoma de Madrid. Ciudad Universitaria de Cantoblanco, 28049 Madrid, Spain
2. Dpto. de Ciencias de la Tierra. Universidad de Zaragoza. C/ Pedro Cerbuna 12. 50009 Zaragoza, Spain.
3. Département de Géologie, Ecole Normale supérieure, Université Hassan II, Casablanca, Morocco
4. Dpto. de Física. Escuela Politécnica Superior. Universidad de Burgos. Avda. Cantabria S/N, 09006 Burgos, Spain.
5. Département de Géologie, Université Moulay Ismail, Meknès, Morocco.
6. Instituto Geológico y Minero de España, Unidad de Zaragoza. C/ Manuel Lasala 44, 9ºB, 50006 Zaragoza, Spain.

Abstract

New magnetic fabric data from 48 sites in Upper Triassic red beds from the Argana, Asni and Tizi n'Tichka areas in the western High Atlas, in combination with rock magnetic analyses, SEM observations and qualitative chemical analyses, reveal that mineralization processes can affect the primary (extensional) or secondary (post-depositional) magnetic fabrics. Twenty out of the 48 analyzed sites show tectonic-related fabrics consistent with the rifting stage (primary). Their orientation suggests that the extensional Atlasic (for the Asni area) and Atlantic (for Argana area) distinct directions prevailing during Liassic times are already present in the Upper Triassic sediments. The other 28 sites show axes switching (including different possibilities, kmax-kmin or kint-kmin), indicating their secondary development related to mineralogical changes after deposition. However, orientation of magnetic susceptibility axes (without considering their relative value) is consistent with the main directions obtained for the rifting stage. This magnetic fabric study also suggests that (i) extension had a small transtensional component and (ii) there is a limited influence of compressional inversion tectonics.

Key words: Atlas, magnetic fabric, extension direction, rift, Triassic

Highlights:

1. Magnetic fabrics of 42% of the sampled sites have primary extensional fabric
2. Secondary magnetic fabric occurs in sites with axes switching or axes tilted with respect to bedding
3. The main carrier is hematite and to a minor extent, phyllosilicates
4. Post-sedimentary hematite hexagonal platelets carry the secondary magnetic fabric

1. Introduction

Magnetic fabric revealed by the analyses of the anisotropy of magnetic susceptibility (AMS) has been proven as a reliable method to unveil petrofabric (Graham, 1954) and hence strain orientation at the time of its development (Borradaile and Tarling 1981; Tarling and Hrouda 1993; Borradaile and Henry 1997; Mattei *et al.* 1997, 1999; Borradaile and Jackson 2004). This method is exceptionally well suited for sedimentary or igneous rocks where phyllosilicates are the main carrier of the magnetic fabric (i.e., marls, marly limestones, clays and ilmenite-type granites) (Mattei et al., 1997; 1999, Cifelli et al., 2004; 2005; 2007; Debacker et al., 2004; Chadima et al., 2006, Bouchez, 1997; Mamtani and Sengupta, 2010). Accordingly, AMS is the only reliable strain indicator where no other mesoscopic petrofabric can be observed. In recent magnetic fabric investigations, the reliability of magnetic fabrics recording and averaging the orientation distributions of minerals has been tested against magnetic and non-magnetic methods to determine the orientation of selected minerals (anisotropy of anhysteretic remanent magnetization AARM, McCabe et al., 1985), anisotropy of isothermal remanence (AIRM, Fuller, 1963; Daly and Zinsser, 1973; Stephenson et al., 1986), X-ray or neutron goniometry (Debacker et al., 2004; Richter et al., 1993; Chadima et al., 2004, 2009; Debacker et al., 2009; Oliva-Urcia et al., 2012).

Magnetic fabrics have also been used to determine the orientation pattern of extensional strain ellipsoids contemporary with sedimentation or early diagenesis in inverted sedimentary basins. To determine strain conditions during the basinal stage, it is necessary to constrain the time of development of the magnetic fabric. Doing so, it can be possible to distinguish the extensional magnetic fabric from the imprint of subsequent compressional events, which may partially, or totally, destroy/erase the extensional magnetic fabric (Soto et al., 2008; Oliva-Urcia et al., 2010a; 2010b; García-Lasanta et al., 2014).

Red beds are excellent rocks to carry out magnetic fabric studies since they contain hematite, a platy mineral having strong magnetocrystalline anisotropy (Morrish, 1994; Martín-Hernández and Guerrero-Suárez, 2012). The AMS of a single crystal is characterized by a minimum principal susceptibility parallel to the crystallographic c–axis and maximum and intermediate principal susceptibility directions on the basal plane (Hrouda, 1980; Guerrero-Suárez and Martín-Hernández, 2012). Because of these properties, examples of compressive magnetic fabrics development in red beds are abundant. These works present the magnetic lineation either perpendicular to the main compression direction or parallel to the tectonic transport direction (Cogné and Gapais, 1986; Cogné and Perroud, 1985; Averbuch et al., 1992; Aubourg et al., 1999, Izquierdo-Llavall et al., 2013).

The succession of extensional and compressional events can produce similar magnetic fabric orientation in red beds when these deformation events are coaxial, i.e a general E-W orientation of the magnetic lineation coherent with an E-W extensional regime is succeeded by a N-S compressional regime, as shown in the Central High Atlas by Moussaid et al. (2013). Another caveat is related to magnetic mineralogies: Saint-Bézar et al. (2002) reported anomalous orientation of AMS axes in red beds (specifically the magnetic lineation) with respect to the tectonic frame in the Eastern High Atlas. These deviations were explained considering that the final magnetic fabric resulted from the intersection of two planar fabrics, the first one related to bedding and to the pigmentary detrital hematite and the second one related to mineralization of goethite occurring in fractures (Saint-Bézar et al., 2002).

This paper investigates the petrofabric of Triassic red beds by means of AMS in order to reveal the tectonic evolution of the western termination of the High Atlas, and, tentatively, to characterize the extensional setting during the first stages of the break-up of Pangea. These results will contribute to constrain the relative weight of the Atlantic (NNE-SSW troughs in present-day coordinates) versus Atlasic (or Tethyan, ENE-WSW troughs) rifting in the Western High Atlas. These two realms were well developed during Early-Middle Liassic times (Jabour et al. 2004) and separated by the Western Moroccan Arch (shallow platform with some emerged parts).

2. Geological setting

The studied area comprises the Argana Basin and the Asni and Tizi n'Tichka areas, located in the Moroccan Western High Atlas (Fig. 1a). The High (ENE-WSW) and Middle (NE-SW) Atlasic systems constitute an intracontinental range that extends from the Agadir Atlantic coast of Morocco (latitude ~32ºN) to the Tunisian Mediterranean coast, for more than 2,400 km. In general, the High Atlas is constituted by Mesozoic basins created during the break-up of Pangea and the opening of the Atlantic and Tethys (Laville and Piqué, 1991; Huon et al., 1993), that were inverted due to the collision of the African and the Eurasian plates from Cretaceous to present times (Mattauer et al., 1977; Jacobshagen et al., 1988; Beauchamp, 1996; Frizon de Lamotte et al., 2000; Teixell et al., 2003; Arboleya et al., 2004). E

xtensional structures of Triassic-Liassic age, mainly N-S but also NNE-SSW faults, segmented by E-W faults, are partly inherited from Paleozoic structures (Laville et al., 1977; Mattauer et al., 1977) and were reactivated during the basinal period (transtension to pure extension) and subsequently during tectonic inversion of the whole basin.

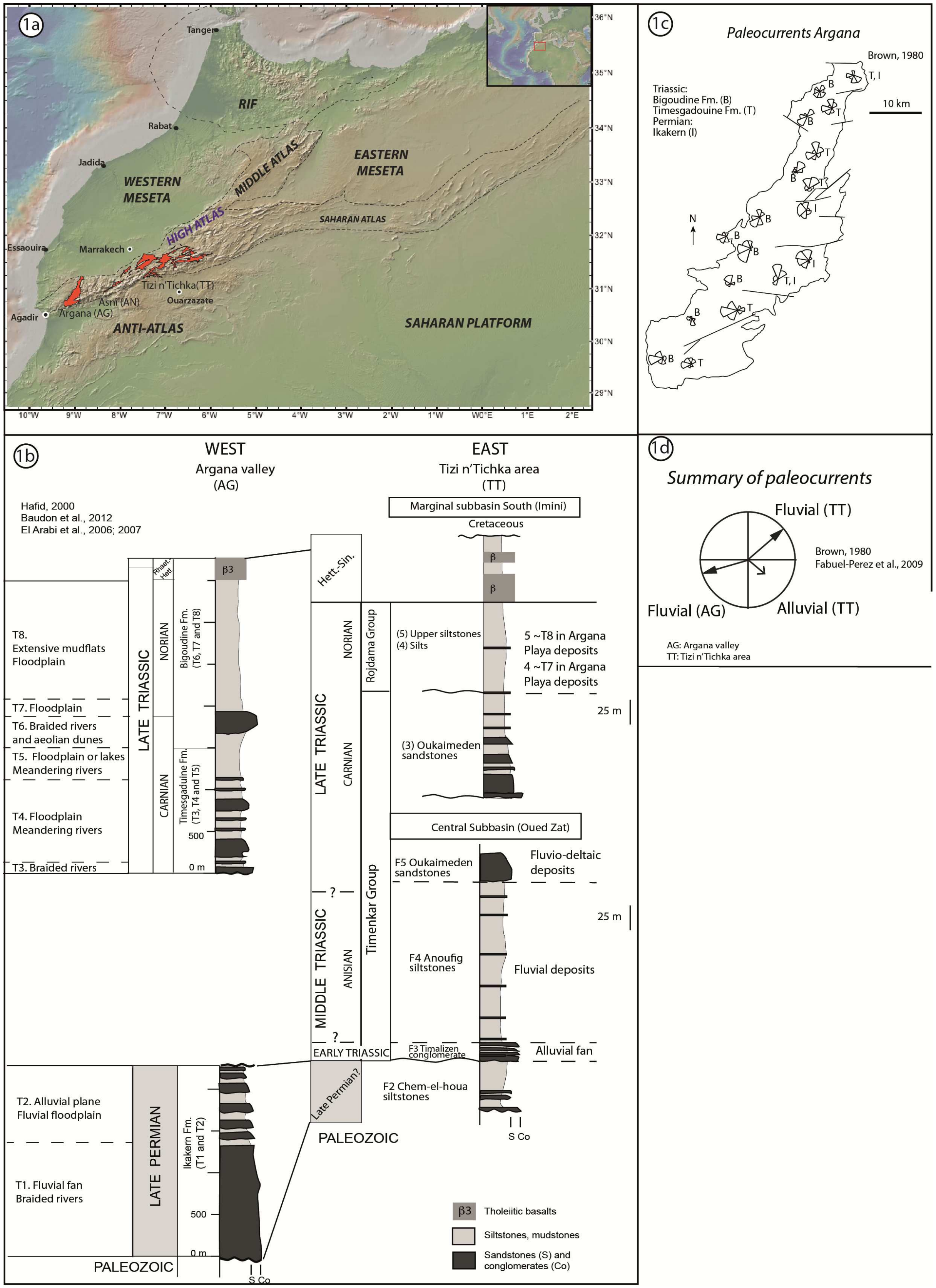

Fig. 1.

2.1. Stratigraphy

The Triassic deposits from the Western High Atlas, particularly in the Argana Basin, consist mainly of fine-grained detrital sedimentary rocks containing basaltic intercalations. In this area, the Triassic sediments overlie Permian and/or older Paleozoic rocks with an angular unconformity. Triassic sediments are more than 3 km thick in the Argana Basin and correspond mainly to deposits of floodplains, mudflats and meandering rivers (Baudon et al., 2012) (Fig. 1b). The thickness of the Triassic sequence is fairly constant along the Argana Basin, representing a package of sediments deposited on the edge of a broader structural domain characterized by slow thermal subsidence, such as a sag basin, or a wide rift (Baudon et al., 2012). Offshore, in the Essaouira basin, the Triassic is represented by salt deposits less than 1 km thick (from cross-sections in Hafid, 2006). To the east of the Argana Basin , in the Tizi n'Test basin, the Triassic sequence overlying the Paleozoic basement is thinner than 500 m (Qarbous et al., 2009). These thickness variations reflect the syntectonic character of the Triassic.

Following Baudon et al. (2012), the Permo-Triassic sediments of the Argana Basin consist of 8 lithostratigraphic units (T1 to T8) grouped in 3 main formations. The upper 6 lithostratigraphic units correspond to the Triassic, which are grouped in two formations i) the Timesgadouine Fm. (T3 to T5), mostly mudstones, siltstones and fine-grained sandstones intercalated with coarse-grained sandstones, deposited in a flood plains with meandering river channels (Brown, 1980) or playa environments with intercalations of sheetflood and ephemeral streams (Hofmann et al., 2000). ii) The Bigoudine Fm. (T6 to T8), corresponding to a distal braided river system grading into aeolian dunes and evaporitic mudflats (Hofmann et al., 2000; Mader and Redfern, 2011; Tourani et al., 2000). Tholeiitic basalts rest unconformably on, or are intercalated with, mudstones of T8 providing an absolute age recalculated to 205 +/- 17 Ma by Fiechtner et al. (1992). These widespread basalt flows are considered to be part of the Central Atlantic Magmatic Province (CAMP, Olsen et al., 2003, in Baudon et al., 2012).

In the Tizi n'Tichka area, the Triassic red beds are grouped in two lithostratigraphic units due to the difficulty in discriminating the four Triassic formations described elsewhere by Biron and Courtinant (1982). This difficulty is related to sedimentary environment variations due to tectonic activity (El Arabi et al., 2006). About 400 m of red beds were deposited during the Middle Anisian, in the northern part of the Tizi n'Tichka area. This age is older than the one considered by Baudon et al. (2012). However, it is necessary to mention that ages for these continental red beds are difficult to constrain (Medina et al., 2001). In the Argana area for example, the ages of T1 and T2 units vary in different studies, ranging from Late Carboniferous to Late Triassic (Baudon et al., 2012 and references therein).

Paleocurrents in the main fluvial systems tend to be oriented towards the WSW in the Argana Valley (Brown, 1980) without a clear maximum (Fig. 1c), and towards the NE in the Oukaimeden Fm. (late Triassic) in the easternmost Tizi n'Tichka sampling area (Fabuel-Perez et al., 2009), Fig.

1d. Alluvial fan currents in the Oukaimaden Fm. are directed towards the SW (Fabuel-Perez et al., 2009) Fig. 1d.

2.2. Structure

Some Paleozoic structures reactivated during the break up of Pangea and also during the Cenozoic inversion. For example, the Tizi n'Test Fault Zone (TTFZ, Fig. 2a), which individualized in Paleozoic times, recorded a polyphase displacement (i) as a dextral transform fault during the Late Carboniferous (Michard et al., 2008), (ii) as main normal fault during the Triassic rifting with a weak shear component according to Qarbus et al. (2003) or (iii) with clear sinistral movement since Carnian times (Proust et al., 1977; Laville and Petit, 1984; Laville and Piqué, 1992) and finally,(iv) as a high-angle reverse fault during the Atlasic compression (Domènech et al., 2015). Other examples are the N-S to NNE-SSW Triassic normal faults (Hafid et al., 2006) in the Western end of the High Atlas and Essaouira Basin (also offshore), that were responsible for the sedimentation of red beds, and follow the same orientation as the West Meseta Shear Zone (WMSZ, Fig. 2a), an area with complex deformation history in Variscan times, particularly during Late Ordovician-Early Devonian tectonic events (Hoepffner et al., 2005; Michard et al., 2008). The trajectory of these N-S to NNE-SSW faults follows the orientation of the Atlantic rifting (Hafid et al., 2006).

Traditionally, Permo-Triassic red beds of the western part of the High Atlas, the Meseta and offshore has been considered to be deposited in graben or half-graben basins having their main faults oriented NNE-SSW to ENE-WSW. These bordering faults were segmented by E-W transfer, strike-slip faults (Mattauer et al., 1977; Hafid, 2000). Basinal history can be summarized in two events: (i) a middle Triassic, NNW-SSE extension resulting in the development of ENE-WSW striking half grabens and (ii) a major Late Triassic to Early Liassic NW-SE extensional phase accompanied by basaltic extrusions and sills. This second phase was responsible for the overall westward-dipping half grabens (Hafid, 2000 and references therein). However, other studies in the Argana area conclude that the NNE-SSW to ENE–WSW faults were not active during the Triassic sedimentation. Medina (1991) identified the overprint of extensional tectonics with two extensional events. The first one affected the Ikakern Fm. (Late Permian, Fig. 2a) leading to the individualization of North-tilted blocks delimited by NE-SW to E-W normal faults resulting from a NNW-SSE regional extensional direction. The second extensional event recorded a change of regional tectonics during the deposition of Bigoudine Fm. (Late Triassic) predating the basalt extrusion. This event is responsible for normal NNE-SSW faults leading to a westward tilting of the Triassic beds in the Argana area indicating a strong influence of the Atlantic rifting. The comparison of these results with other

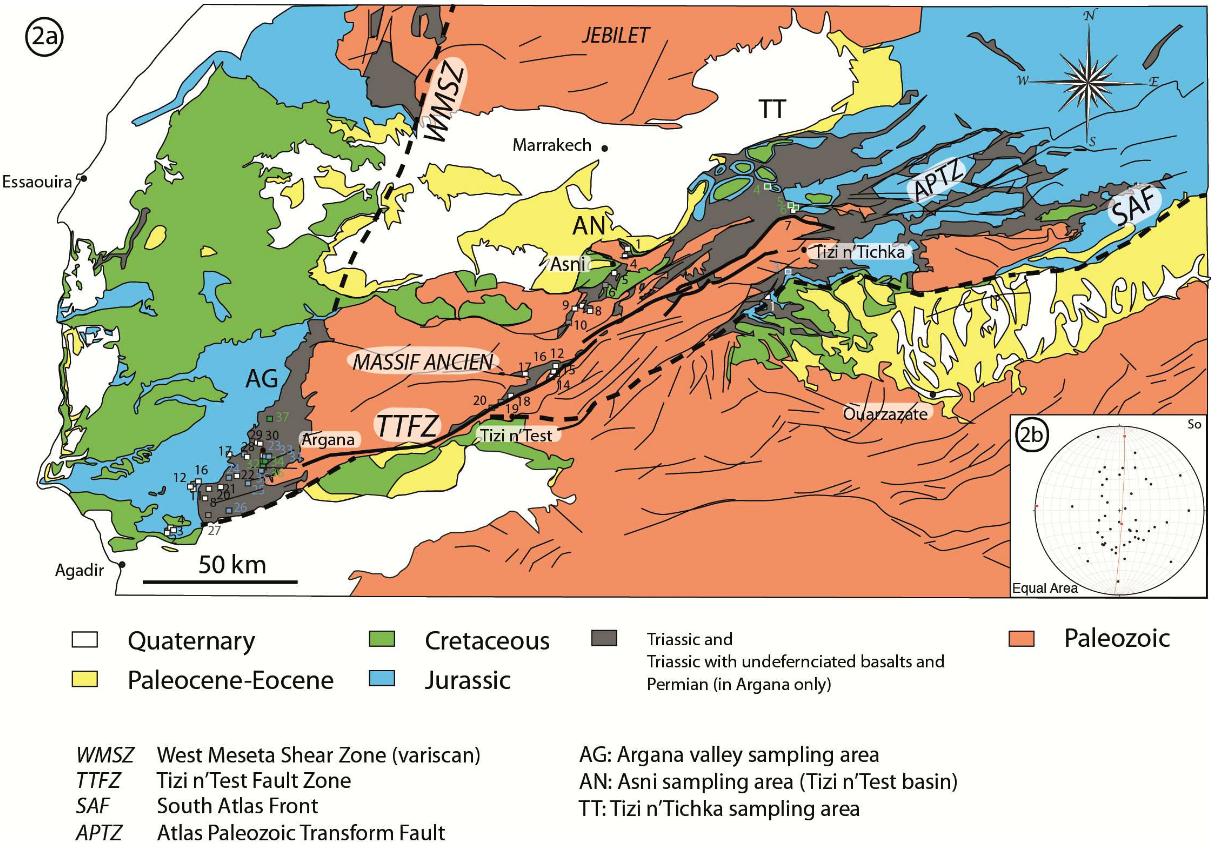

Fig. 2.

Permo-Triassic basins in the Atlantic margin and in the High Atlas suggested that the structural evolution in the western part of the High Atlas has been mainly affected by Atlantic rifting (Baudon et al., 2012 and references therein).

The dismiss of the transtensional opening of the Triassic basins (Petit, 1976) in favor of purely extensional tectonics (Medina and Errami, 1996) was already considered by Qarbous et al. (2003) after studies of the Triassic microstructures of the Tizi n'Test Basin located to the east of Argana Basin and along the Tizi n'Test Fault Zone. Qarbus et al (2003) differentiate between Atlantic rift (coastal basins with NNE-SSW orientations, such as Essaouira and Argana), and Atlasic (or Tethyan) basins such as the Tizi n'Test basin, having ENE-WSW orientation. They also conclude that strike-slip component along the TTFZ is minimal or absent. In addition, they described only one main NW-SE Triassic extension direction (El Wartiti et al. 1992; Aït Brahim and Tahiri 1996; Medina, 2000, Qarbous et al. 2003).

3. Methodology

A total of 48 Triassic red beds sites were drilled in the field with a portable, gasoline-powered drill machine. Eight to ten cores were taken and oriented at each site (Table 1) obtaining a total of 758 specimens (16 per site in average). Attitude of bedding, brittle structures (fractures and faults) and paleocurrents (laminae in planar cross-bedding) were also measured. Sites are distributed in three areas, named respectively AG, TT and AN in figure 2a: i) the Argana valley in the west (26 sites), ii) Oukaimede-Ourica area in the east, near Tizi n'Tichka (6 sites), and iii) Asni area in the middle, in the Tizi n'Test fault zone area (16 sites). Structural analysis at the mesoscale is often difficult in the Upper Triassic because solution-precipitation processes responsible for the formation of kinematic indicators in faults, commonly found in calcareous rocks, are rare in detrital rocks (Petit, 1987). Under these conditions the approximate orientations of the principal axes of the paleostress ellipsoid can be obtained considering (i) simple models of stress-faulting relationships (Anderson, 1951; Ramsay and Huber, 1987 and references therein) and (ii) that in extensional settings fractures and joints are often parallel to the main normal faults (see e.g. Hilley et al., 2001) and/or perpendicular to the minimum horizontal stress axis (Hancock, 1985), Conversely to brittle mesostructures, AMS provides a tool that can be used at a regional scale with limitations derived only from magnetic mineralogy and exposures. The new AMS data in combination with the previous structural data can help deciphering the main petrofabric orientation related to the main extension direction in Triassic times.

3.1. AMS at room (RT-AMS) and low (LT-AMS) temperature

Magnetic susceptibility is a physical property of all materials and represents their capacity to be magnetized in a given magnetic field. The magnetic susceptibility (K) is described by a second-rank tensor that relates the applied magnetic field (H) to an induced magnetization (M): M = K * H. AMS in rocks depends mostly on crystallographic preferred orientation, shape of grains, composition and, sometimes, interaction of magnetic minerals (Tarling and Hrouda, 1993).

Measurements of AMS at room (~25ºC, RT-AMS) and low (~77 K, LT-AMS) temperature were done at the magnetic fabrics laboratory of the University of Zaragoza (Spain). A KLY-3S (AGICO Inc.) was used to perform the measurements at operating frequency of 875 Hz and field of 300 A/m. The second rank tensor of the AMS is graphically displayed by a three-axes ellipsoid (kmax > kint > kmin) described by its principal directions, shape and degree of anisotropy or eccentricity. The Anisoft 4.2 software (Chadima and Jelinek, 2009) was used to calculate the principal susceptibility axes in order to determine the orientation of the magnetic ellipsoid. Their shapes were described using the shape parameter T, whereas their anisotropy degree was established using the corrected anisotropy degree Pj (Jelínek, 1981). Oblate ellipsoids (planar, $0<T<1$) show large kmax and kint axes, and small kmin axes, whereas prolate ellipsoids (linear, $-1<T<0$) show large kmax and small, similar kint and kmin axes. Neutral ellipsoids show similar magnitudes for all axes. The magnetic lineation is the clustered orientation of the kmax axes, whereas magnetic foliation is the plane perpendicular to the kmin axes and hence, contains kmax and kint.

The analyses of the AMS at low temperature enhance the paramagnetic susceptibility, following the

Curie-Weiss law $k_{para} = C / (T - \theta)$, where C is the Curie constant, T temperature and θ is the paramagnetic Curie temperature. The enhancement of the paramagnetic signal at low temperature occurs because the diamagnetic susceptibility and, to a first approximation, ferromagnetic susceptibility below the Curie point, are independent of temperature. Since the pioneering work by Richter and van der Pluijm (1994) many studies have used LT-AMS. In this paper we use the Lüneburg et al. (1999) approach, where samples are cooled down in liquid nitrogen (~77 K) and measured in air. Specifically, the specimens were immersed in liquid nitrogen for one hour prior to start measurements in air. Between changing positions according to KLY-3S procedure (3 positions), samples were immersed again in liquid nitrogen for 10 min. This procedure has been tested in marls and marly limestones, with enhancement at LT of 2 to 2.8 times the RT bulk susceptibility (Lüneburg et al. 1999, Oliva-Urcia et al., 2010, García-Lasanta et al. 2014). Repeated measurements of the same sample provide similar results.

3.2. Magnetic mineralogy

Thirteen selected samples were crushed to powder in order to perform thermomagnetic analyses to obtain information about the ferromagnetic s.l. minerals present. The variation of magnetization or magnetic susceptibility with temperature (M-T or κ-T curves) allows the identification of magnetic phases based on their Curie or Néel temperature, which defines the transition from ferromagnetic s.l. (TC) or antiferromagnetic (TN) to paramagnetic ordering.

One set of κ-T analyses was done at the KLY-3S in conjunction with a CS3 furnace that allows a temperature range from room temperature to 700ºC with a rate of 11ºC per minute. A protective Ar atmosphere prevents from oxidation during heating-cooling runs. The Cureval 8 software (Chadima and Hrouda, 2009) substracts the empty furnace signal and allows calculating automatically the inverse of the susceptibility (1/k) in order to determine the change from ferromagnetic to paramagnetic behavior (Petrovsky and Kapicka, 2006).

In addition, the variation of magnetization with temperature was also analyzed using a variable field translation balance (MMAVMFTB, Petersen Instruments) in the Paleomagnetic Laboratory of the University of Burgos (Spain). Analysis of the curves (calculation of the TC or TN) and the calculation of the parameters of the hysteresis loops (H: coercivity, Ms: saturation magnetization, Mrs: magnetization in the absence of a magnetic field) were done with the program RockMagAnalyzer 1.0 (Leonhardt, 2006). The magnetization-temperature curves are performed under a 381 Oe field.

In addition, measurements of the acquisition of the remanence magnetization (IRM) and the thermal demagnetization of IRM (Lowrie, 1990) in three perpendicular axes of decreasing magnetic field were also performed in 5 selected standard samples (2.5 cm diameter x 2.1 mm height cylinders).

3.3 SEM observations

Back scattered electron images were obtained from thin sections of 2 different selected sites with a Field Emission Scanning Electron Microscope (FESEM) at 20 kV at the University of Zaragoza. Semiquantitative EDX analyses were performed with the INCA microanalyses software (Oxford Instruments). A piece of cobalt standard was used to calibrate the EDX signal at the beginning of every SEM session. The samples were cut parallel to bedding (S0), and were previously carbon coated.

4. Results

4.1. Field observations

The overall structure of the Argana area shows E-W asymmetric, gentle folds (Figs. 2b and 3) having shallow dips in their back limbs, and steeper dips in their front limbs, that are linked to re-activation of normal faults (Fig. 3a, b, d, e). In some cases, small-scale buttressing against normal faults can be also observed (Fig. 3c, f). Towards the East, the Triassic units overlying the Palaeozoic show a shallow westwards dip. Structures are more complex in the other studied areas (Asni and Tichi n'Tichka) where re-activation of faults involving the Paleozoic and the Triassic rocks, and shear bands indicating sinistral strike-slip motion can be seen.

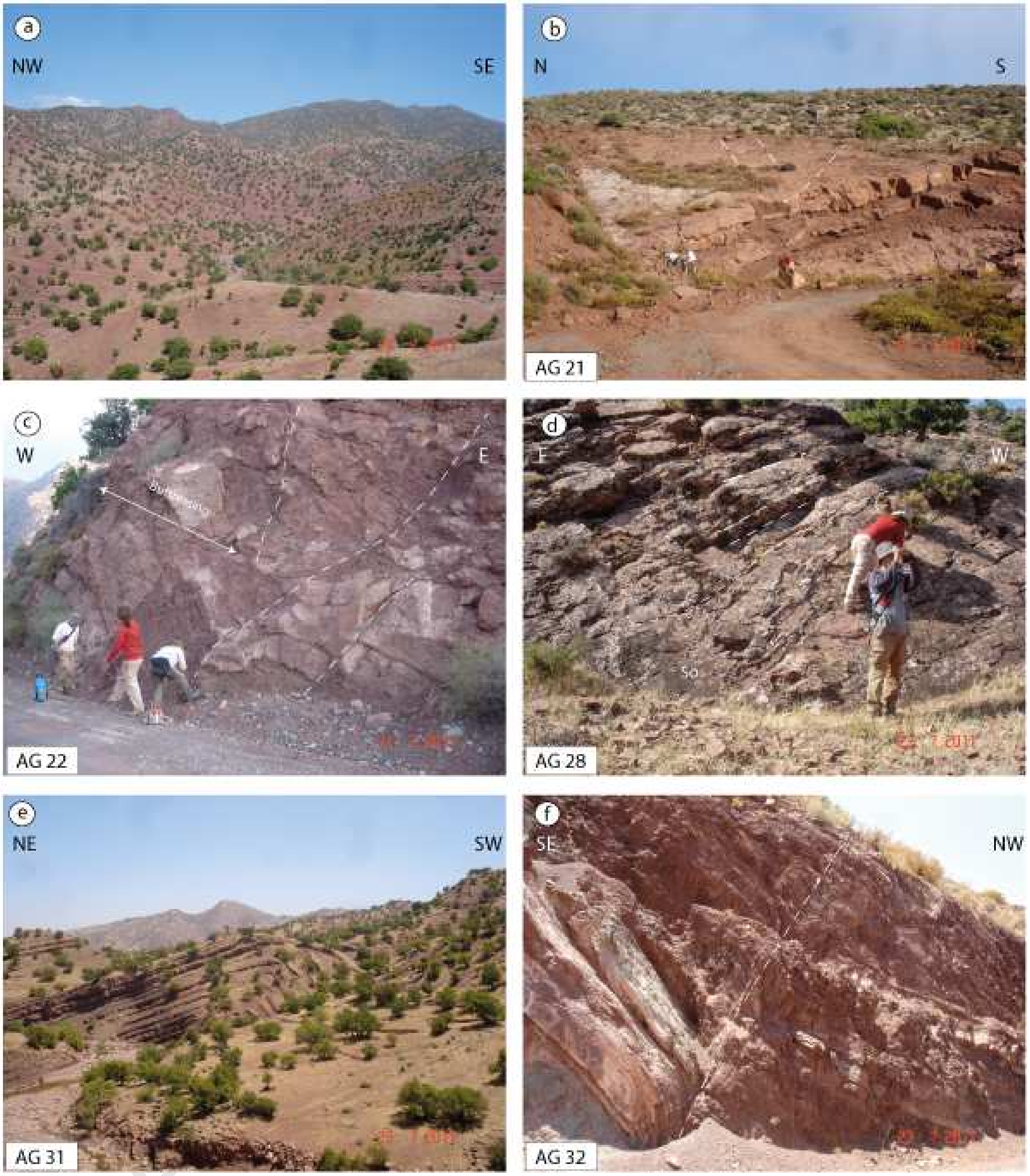

Fig. 3.

At the outcrop scale, numerous normal faults and fractures inherited from the extensional stage can be recognized (Figs. 4c, d, f, g). In some of them the syn-tectonic origin of faults can be assessed from the changes in thickness of the involved sedimentary units (Fig. 4d). Faults are either isolated or forming conjugate sets that define Andersonian models (Figs. 4e, g, h). A common feature is the presence of sets of extensional fractures sub-parallel to the main set of faults in each outcrop (Fig. 3d, Figs. 4b, c). Less frequently, fractures can be related to strike-slip conjugate systems probably resulting from the re-activation of tension fractures inherited from the extensional stage.

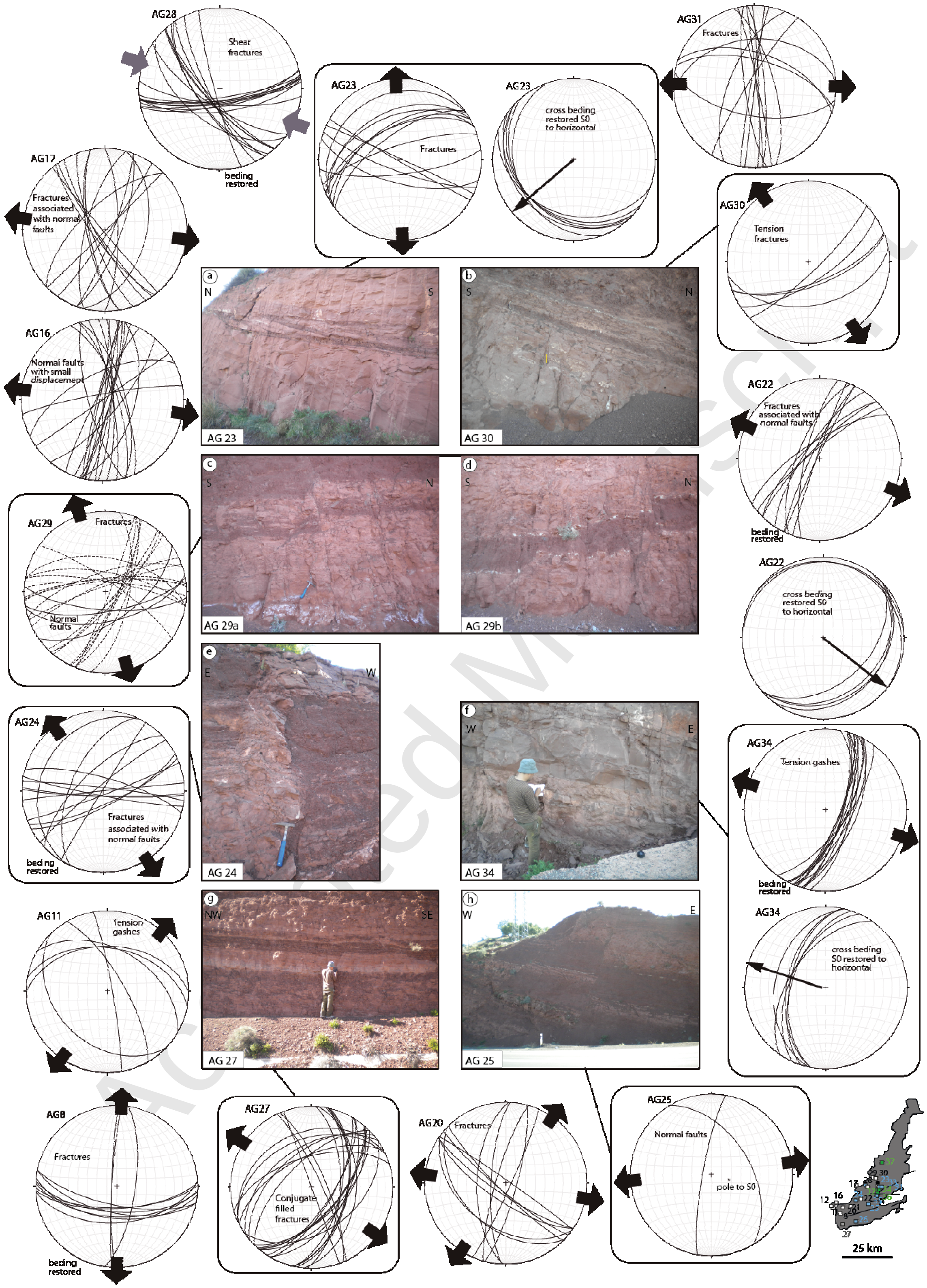

Fig. 4.

Directional analysis of faults (Fig. 4) indicates a dominant NNE-SSW to ENE-WSW direction in most of the analyzed outcrops, and extension directions inferred from normal fault systems (mostly conjugate normal fault systems and tension fractures associated with normal faults) range between

WNW-ESE and NNW-SSE. The lack of kinematic indicators on fault planes precludes, however, obtaining more accurate stress direction and the Shmin inferred can only be considered as approximative.

4.1. AMS at room temperature (RT-AMS)

Average values of the bulk susceptibility per site range between 41 x 10^{-6} SI and 543 x 10^{-6} SI, with a total average of 147 x 10^{-6} SI (standard deviation of 116 x 10^{-6} SI, Fig. 5). The dominant shape fabric is oblate to neutral except for 10 sites, which have negative T values (prolate shapes). The corrected anisotropy degree (Pj), is lower than 1.07 in all but four sites. The lack of dependence between the anisotropy corrected degree and the mean susceptibility indicates that the magnitude of the magnetic ellipsoid is not directly controlled by magnetic mineralogy (Table 2).

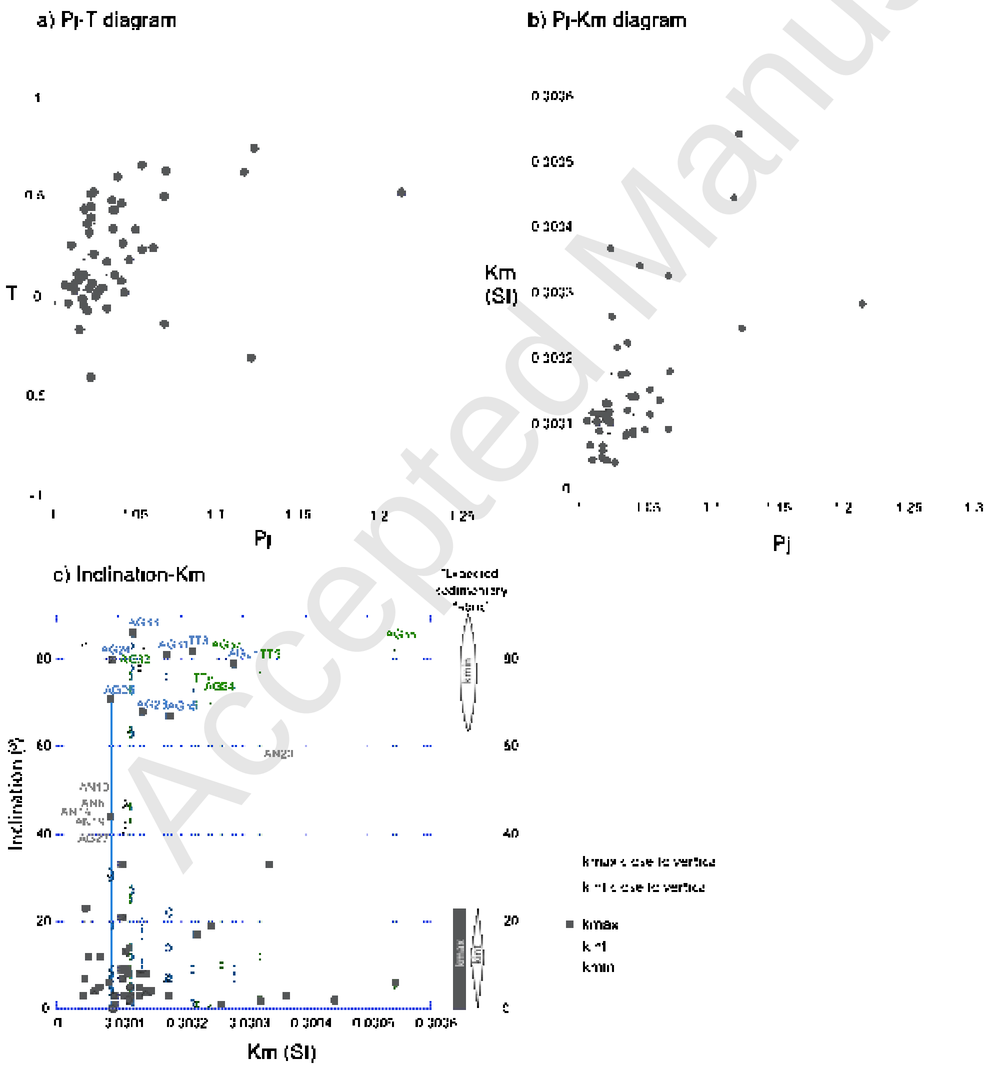

Fig. 5.

In the red beds from the western sector of the Moroccan High Atlas, four types of fabrics can be found, regarding the disposition of the magnetic ellipsoid axes respect to bedding (Figs. 5c and 6a):

i) Magnetic fabrics keeping their *a priori* sedimentary disposition, that is, kmax and kint axes are within the bedding plane and kmin axes are perpendicular to it (28 sites, black numbers in Table 2).

ii) Magnetic fabrics showing an interchange between kmax and kmin axes; kmax axes are perpendicular to the bedding plane and kmin axes are on the bedding plane (blue names and bars in Table 2 and Fig. 5c, totaling 8 sites).

iii) Magnetic fabrics having kint axes perpendicular to bedding and kmin axes within the bedding plane (interchange between kint and kmin axes, green names and bars in Table 2 and 2 and Fig. 5c, totaling 6 sites).

iv) Intermediate position of the axes: in four cases out of six, kmax axes are within the bedding plane and kint and kmin axes are oblique to it. In the other two sites, kmax axes are also tilted respect to bedding (grey names in Fig. 5c).

The clustering of the magnetic ellipsoid axes is well defined, i.e., confidence angles provided by the calculation of the average are lower than 34º except for 12 sites, where kint and kmin axes (in 7 sites) or kmax and kmin axes (5 sites, Fig. 6b) show girdle distributions. Those 12 sites belong to fabric types i) to iv).

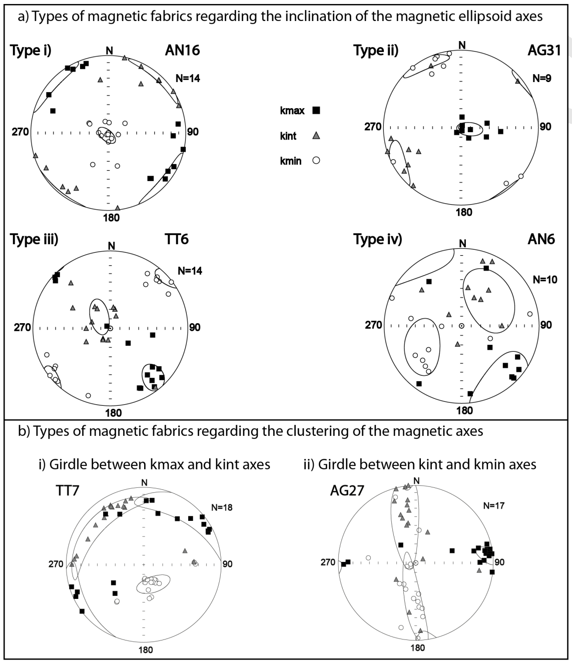

Fig. 6.

4.2. AMS at low temperature (LT-AMS)

Ten sites were selected in order to perform AMS measurements at low temperature (~77 K). Between 6 and 8 samples per site were analyzed, except in TT3 site, where only 5 samples were measured (Table 3).

The average ratio of magnetic susceptibility at LT respect to RT varies between 0.74 (AG36 site) and 2.33 (AN7 site, Table 3). Comparing sample by sample (see Fig. 7a), most values lie between 1.5 and the perfect paramagnetic behavior (3.8). LT/RT values are particularly low for AG36, TT5, TT3 sites and some samples of AG28 and AG24 sites.

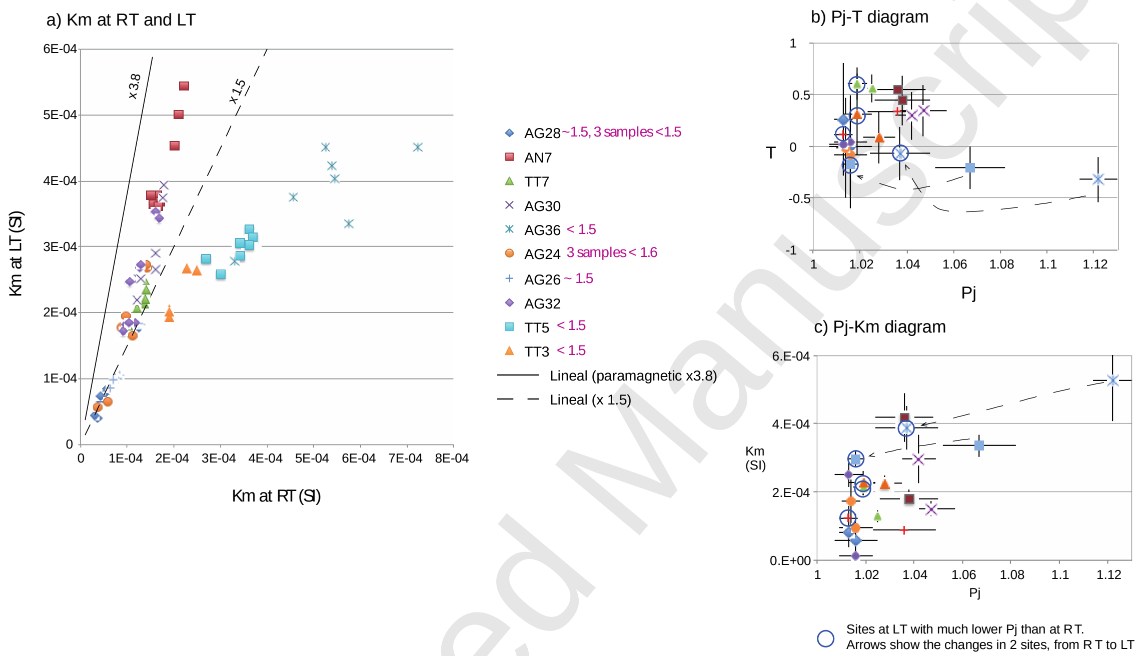

Fig. 7.

Samples with low LT/RT ratios, indicating little contribution of paramagnetic minerals to the magnetic susceptibility, also show a decrease in the standard magnetic lineation (L) and the corrected anisotropy degree (Pj) values at low temperature respect to the room temperature values, due to the interchange in the magnetic axes below the Morin transition of the main magnetic carrier, i.e. hematite (Fig. 7b and c).

The measurements at low temperature (LT) are focused inmagnetic fabric types i) to iii), where sedimentary fabrics (type i) or axes switching (types ii and iii) are found. Sites with different magnetic susceptibility values were also examined at LT (Fig. 8). Comparing the orientation of the magnetic ellipsoid at room (RT) and low (LT) temperatures, it is interesting to note that there are three sites belonging to type i) where the ellipsoid is similarly oriented at both temperatures regardless the LT/RT ratio: AN7 (having the highest LT/RT ratio), AG36 (having the lowest LT/RT ratio) and AG30 (stereoplots in Fig. 10).

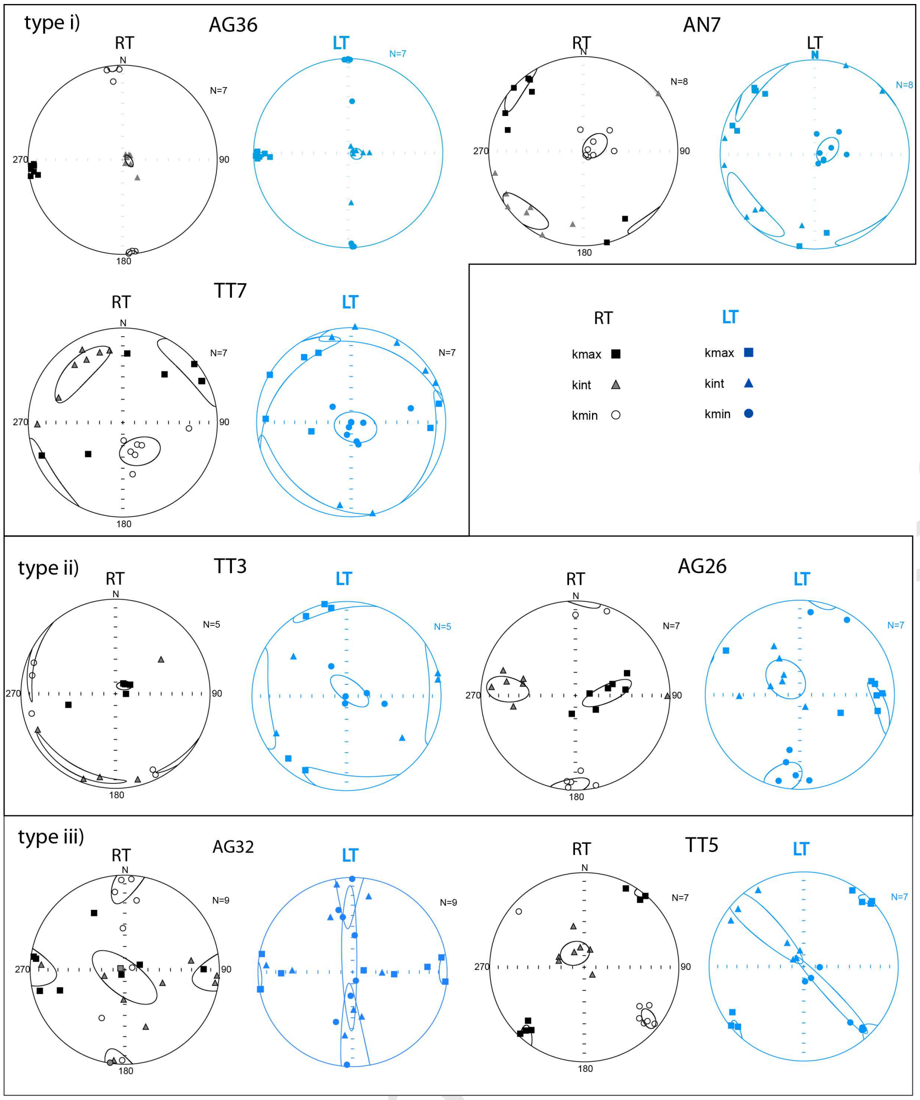

Fig. 8.

Another example of type i) is site TT7, where orientation of the kmin axes at LT appears closer to the bedding pole, and kint and kmax scattered within the bedding plane. However, for type ii) results differ: one site (TT3, with LT/RT ratio lower than 1.5) shows interchange of magnetic axes: kmin axes at LT coincide with kmax axes at RT. This behavior is typical of SD magnetite, siderite and ferroan carbonates (inverse fabrics, Rochette, 1987). However, in AG26 (another example of type ii), having LT/RT ratio close to 1.5), kint axes at LT occupy the position of kmax axes at RT.

Finally, in two sites of type iii) having different LT/RT ratio (AG32 > 1.5 and TT5 < 1.5) only some samples interchange positions at LT: some kmin axes at LT coincide with kint axes at RT, but kmax axes remain in the same position at RT and LT. As a result, the average position of the axes at LT appears tilted with respect to bedding (Fig. 8).

4.3. Mineralogy

The thermomagnetic curves reveal the predominance of different ferromagnetic s.l. minerals depending on the technique used (Fig. 9). The κ-T curves (temperature-dependent magnetic susceptibility curves) suggest the predominance of magnetite as ferromagnetic mineral, with some new formation above 400ºC, especially in three samples (AG23, 24 and 25). Only one sample out of 9 (AN7) shows unequivocally the predominance of hematite (T of the 1/k curve is ~ 650º C), although hematite is present in 5 samples (AG32, 28, 30, 36, TT7) together with magnetite (temperatures of 1/k are 580º C for magnetite and between ~656ºC and 680ºC for hematite). However, the same samples analyzed in the variable field translation balance, reveal the predominance of hematite as ferromagnetic s.l. mineral, as inferred from: i) M-T curves (final decay of the magnetization well above 660ºC), ii) acquisition of the isothermal curve (IRM), which does not reach saturation at the maximum applied field (750 mT) and iii) back-field experiment, where the coercivity of the remanence is below -300 mT (except AG24 and AG28, with Bcr < than 178 mT). Only AG24 shows a soft coercivity component in the IRM acquisition curve and back-field (Fig. 9). The enhancement of the magnetite signal in the κ-T curves seems to be related to the reduction of Al substituted hematite under the presence of phyllosilicates (illite, chlorite, kaolinite, Ca-montmorillonite) as seen in Jiang et al. (2014) and then to the higher magnetic susceptibility (two orders of magnitude) of magnetite respect to hematite. The three components IRM performed in standard size samples confirm the predominance of hematite as the main ferromagnetic mineral present (Fig. 9).

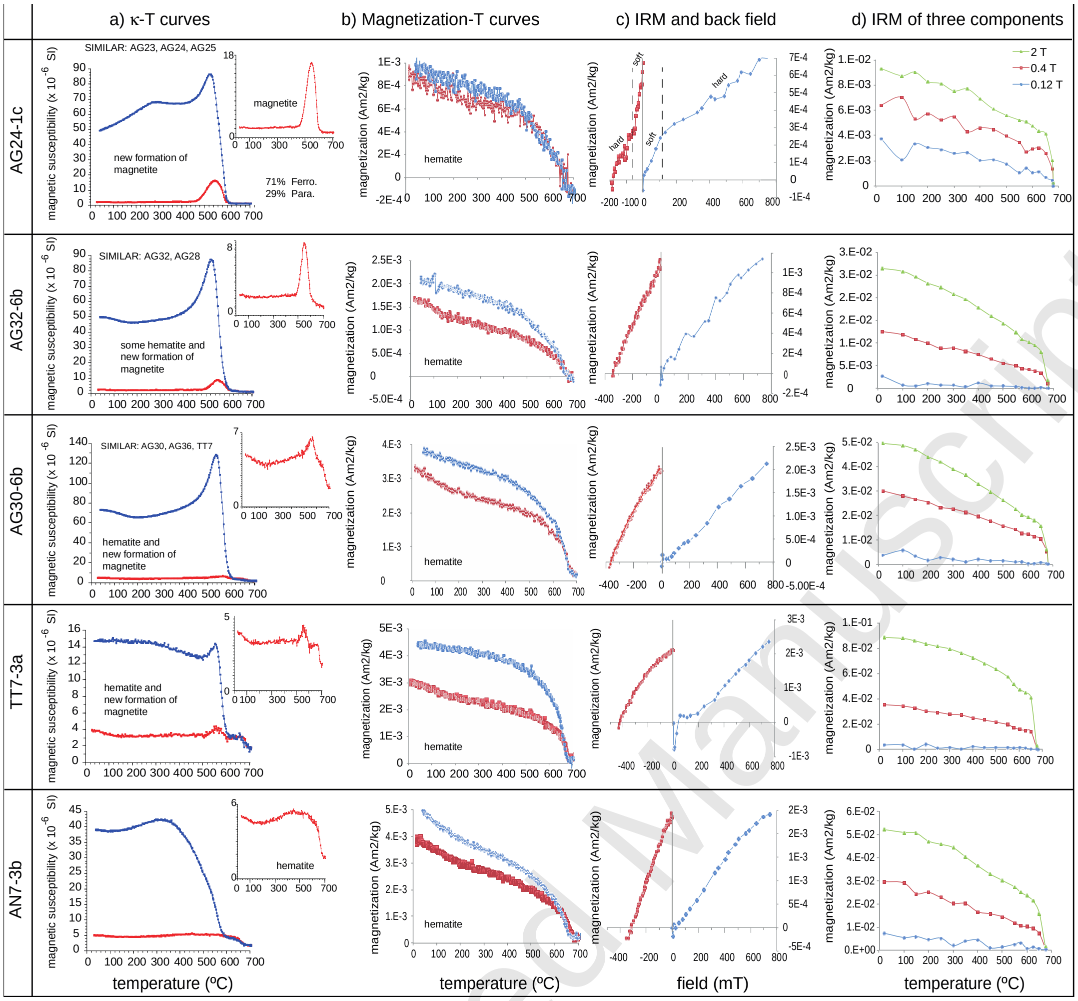

Fig. 9.

4.4. SEM observations

Two selected samples were analyzed under the electron microscope. One is AG30, which shows a magnetic fabric with kmin axes perpendicular to bedding plane and kmax and kint axes located on the bedding plane. At LT and RT ellipsoids overlap and LT/RT average ratio is ~ 2. The other sample is AG24, which shows kmax axes perpendicular to bedding and kint and kmin axes on the bedding plane at RT. At LT, samples with a LT/RT ratio closer to 2 (four samples out of seven) show their kmin axes perpendicular to bedding (kmax and kint axes within the bedding plane), whereas the samples with lower LT/RT ratios maintain their kmax axes perpendicular to bedding even at LT (shown in red in Fig. 10).

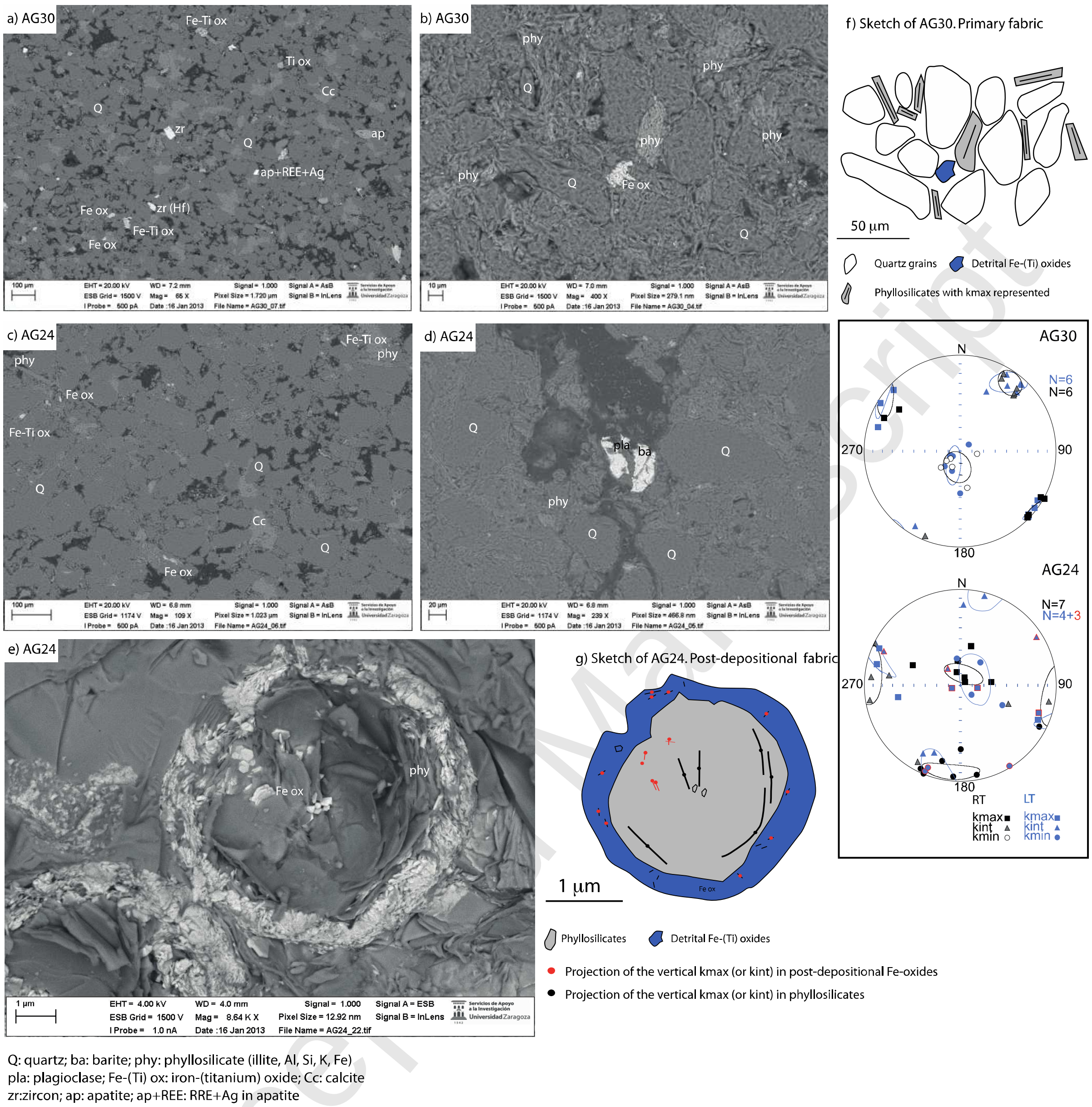

Fig. 10.

Both samples show rounded and elongated quartz grains (50-100µm) as groundmass mineral, with minor quantities of other silicates: plagioclase (~ 40 µm), elongated phyllosilicates (10 to 200 µm in size, probably illite), and rounded calcite grains (~ 60 µm). As opaque minerals there are detrital iron and iron-titanium oxides, titanium oxides, and zircon, all of them with a size range of 20 to 70 µm. In addition, apatite (~45 µm) and interstitial barium sulphate (barite, ~ 10 to 70 µm in size) are also found. Flat iron oxides (< 1 µm) with hexagonal habit, which is typical of hematite, are also present in AG24; they appear forming a circular structure around phyllosilicates. Additionally, light rare earth elements (La, Ce, Nd) with Ag and Fe are detected in detrital apatite, and Hf appears within zircon in AG30 (Fig. 10).

5. Interpretation and discussion

5.1. Timing of formation and carriers of the magnetic fabric

In order to use magnetic fabric measurements to define the petrofabric and to infer the strain pattern during its formation, two intertwined key points are to determine i) the time of development of the magnetic fabric and ii) the main mineral phase carrying the AMS. When magnetic fabric develops at early stages of sedimentation/diagenesis ("sedimentary" fabric), it reveals the strain pattern at that time, provided that no subsequent processes affect its primary orientation (Mattei, 1997; 1999; García-Lasanta et al., 2013). Sedimentary fabrics normally show kmax and kint axes contained on the bedding plane, whereas kmin axes will be clustered at its pole. Subsequent geological processes (changes in the extensional stress field orientation, compression, new mineralizations) can change the disposition of the magnetic ellipsoid with respect to bedding.

As revealed by magnetic mineralogy experiments, the main ferromagnetic s.l. mineral present in the studied samples is hematite. From low temperature experiments, it is known that magnetic susceptibility of hematite decreases between 50 to 90% at LT with respect to RT for fractions of pure hematite (see κ-T curves in De Boer and Dekkers, 2001). Measurements of magnetic susceptibility of hematite at ~77 K are performed below the Morin transition (Morin, 1950), which occurs at ~ 260 K (Özdemir et al., 2008 and references therein). The Morin transition (TM) is not related to a crystallographic change (as occurs for the Verwey transition in magnetite) but to the isotropic point. The first hexagonal magnetocrystalline anisotropy constant (K1) of hematite is negative above TM and positive below it (Morrish, 1994). Below TM, the easy directions of magnetization changes, resulting in a reorientation of the antiferromagnetically coupled atomic spins from the basal plane for T> TM to the hexagonal c-axis for T< TM (De Boer and Dekkers, 2001 and references therein). The low-field susceptibility below TM consists only of the antiferromagnetic susceptibility and a superimposed susceptibility in the direction of the c-axis arising from defects in the hematite lattice. Below TM, only a small proportion, if any, of domain walls are observed (Morrish, 1994), and thus the displacement of domain walls in formerly PSD and MD grains no longer contributes to the low-field susceptibility (De Boer and Dekkers, 2001). The magnetic susceptibility increases with increasing grain size (Dankers, 1978; Collinson, 1983). The transition becomes completely suppressed either when pure hematite grains are smaller than 0.02–0.03 μm (e.g. Bando et al. 1965; Kündig et al. 1966) or when critical quantities of impurity cations are incorporated in the hematite lattice (e.g. Morin 1950; Flanders Remeika, 1965). Consequently, the weakly ferromagnetic phase persists in these hematite grains through the whole temperature range down to 4 K (De Boer and Dekkers, 2001).

The LT/RT ratios suggest the presence of phyllosilicates (paramagnetic signal) in addition to hematite as main carriers of the magnetic susceptibility in most of the samples. Only in AG36 and

TT5 sites, which show lower susceptibilities at LT than at RT (as expected for hematite, since susceptibility decreases at temperatures below TM), the contribution of paramagnetic minerals is negligible.

The variations in the orientation of the magnetic ellipsoid at LT compared to RT can be due to either the influence of the paramagnetic minerals in the paramagnetic-enriched samples, or the change through the isotropic point of hematite (change of orientation in the “easy” axis of magnetization, on the basal plane above TM and on the c-axis below TM, Morrish, 1994; De Boer and Dekkers, 2001), or alternatively it can be a mixture of both.

Considering the optical and chemical SEM analyses, two significant observations are noticeable: the first is the new formation of iron oxides (hematite), promoting a secondary fabric that may affect the original signal, and the second is the presence of barite as interstitial fillings in pores and fractures, which indicates running of mineralized fluids after compaction and fracturing. The temperature of mineralizing fluids ranges between 100ºC to 350ºC for barite precipitation (Guilbert and Park, 1986) under stable reducing conditions (Muzio et al., 2013). The hexagonal flat shape of hematite < 1 μm, arranged in circular structures and surrounding phyllosilicates, indicates a post-sedimentary origin. The distribution of these newly-formed hematite grains can explain the post-sedimentary magnetic fabric record in types ii) to iv) (sketches in Fig. 10). Connecting the two events together: new formation of barite and iron oxides involves the input of fluids enriched in S, Ba and Fe that would agree with the event also proposed by Saint-Bézar et al. (2002) in the Eastern High Atlas (Goulmina city area). These authors inferred a relationship between unusual tectonic fabric orientation where the magnetic foliation is oblique to bedding and fluid flow along fractures developed during basin inversion, as for example, conjugate or single, pervasive sets of fractures at the limbs of folds (Figs. 3b, d). However, new formation of hematite at the latest stages of diagenesis (prior to lithification) cannot be discarded with the available data.

As pointed out in the introduction, the angular relationship of the magnetic axes with the bedding plane is the first observation to consider in order to discard sites with secondary fabric or a mixed signal (primary plus secondary). In a regular sedimentary fabric, kmin axes are perpendicular to bedding and kmax and kint are contained within the bedding plane (Tarling and Hrouda, 1993). In extensional settings, kmax axes are parallel to the extension direction (commonly perpendicular to the strike of main normal faults) on the bedding plane (Mattei et al., 1997, 1999; Cifelli et al., 2005). This scenario can be subsequently transformed due to changes in the stress regime, i.e., different extension direction or compressional stages, and also by new mineralizations developing under different tectonic settings (Housen and van der Pluijm, 1990; Parés et al., 1999; Aubourg and Robion, 2002; Hirt et al., 2004; Oliva-Urcia et al., 2009 among others). Therefore, the original extensional setting of the magnetic fabric can be partly or definitely masked by these subsequent events.

Consequently, RT magnetic fabric types ii) to iv) in the red beds of the western High Atlas are probably recording a secondary fabric acquired in subsequent events related to mineralogical changes and formation of new minerals, since kmax and kint axes are not contained within the bedding plane or kmin axes are not perpendicular to bedding plane (Fig. 11). Conversely, magnetic fabric type i) can be interpreted as a primary fabric without the overprint of later mineralogical artifacts. However, the coincidence in the orientation of axes in all types indicates a relationship with the primary fabric, possibly because mineralizations during subsequent events is conditioned by the original mineralogical fabric (Fig. 6).

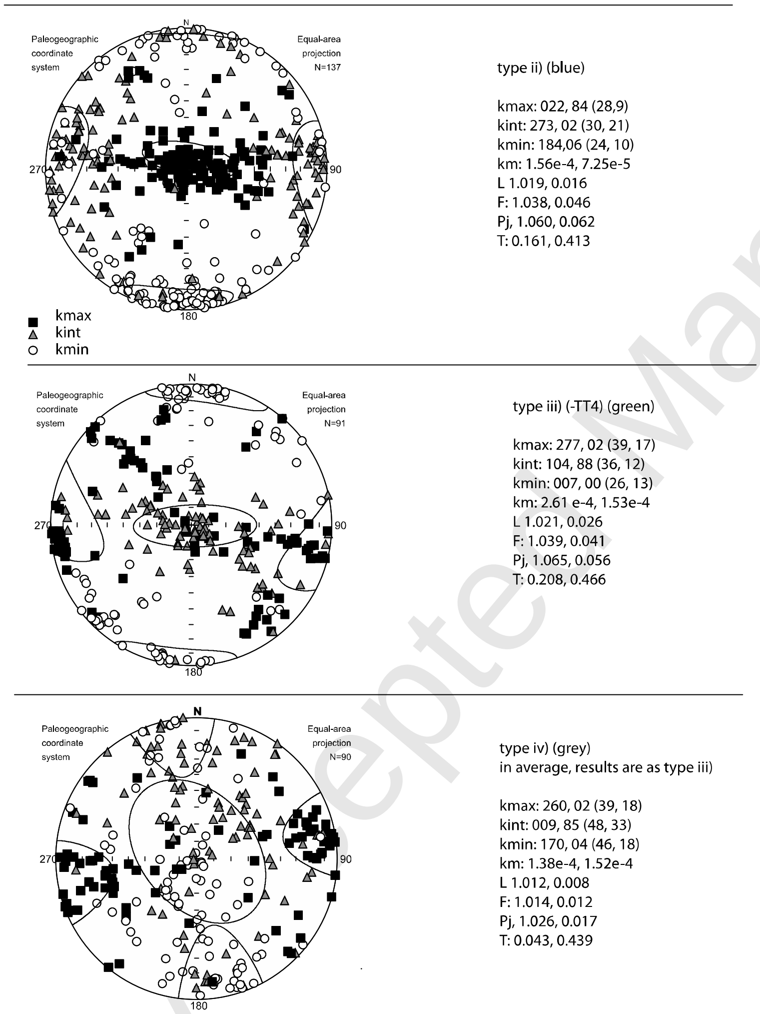

Fig. 11.

Structural data at the scale of the sampled sites provide insights about stretching directions (Shmin), which in particular sites (AG 11, 16, 17, 22, 25, 27, 29, 30 and 34, Fig. 2a) are more reliable than in others, due to the type structures present at the outcrops (tension gashes, conjugate normal fault systems or fractures closely related to normal faults). Comparing those stretching directions with the magnetic lineation (Table 2), there is certain overlapping in 6 cases. Therefore, in spite of the scarcity of outcrop-scale structures, a good correlation can be established between the magnetic fabric signal and the extension directions obtained from structural data.

5.2. Structural interpretation of the primary magnetic fabric

Considering in first instance the sites with primary fabric, having kmin perpendicular to bedding and kmax and kint within the bedding plane, and, within this set, the sites with clustered kmax withconfidence angle lower than 34º, 20 sites out of 48 (42%) can be used to determine the extensional tectonic regime at the time of deposition of the red beds (Middle-Late Triassic). These particular sites are located in AG area (12 sites) and AN area (8 sites) (in Fig. 12, all sites having horizontal kmax axes are presented once bedding is restored to horizontal).

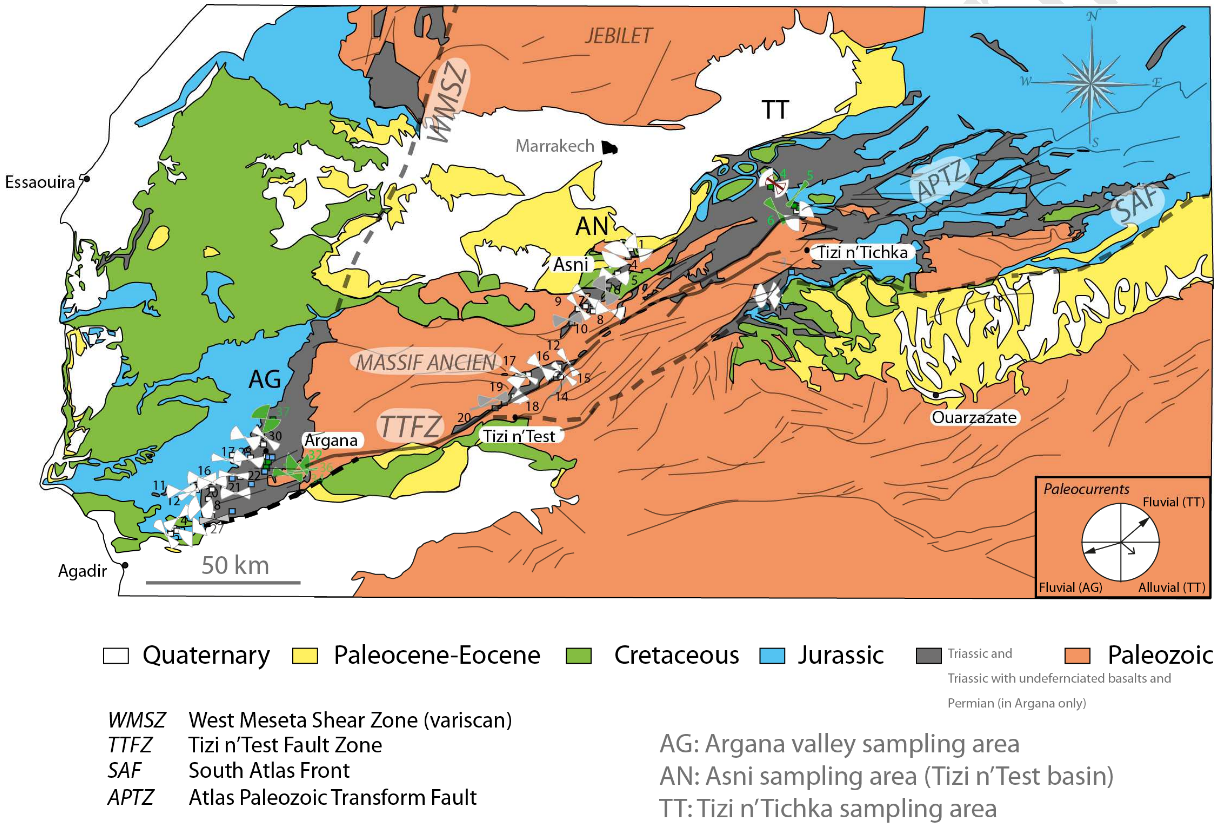

Fig. 12.

Primary or sedimentary fabrics can be modified during the subsequent deformational stages, especially if formation of cleavage or new mineral phases are involved (i.e., Housen and van der Pluijm, 1991; Housen et al., 1993; Debacker et al., 2004; Oliva-Urcia et al., 2013). Penetrative deformation in the High Atlas is restricted to the Lower-Middle Jurassic outcrops in its central zone, where axial planar cleavage related to anticlines and close to outcrops of igneous rocks has been described. Timing of such deformation is in dispute: some authors consider it to have a Jurassic age (Schaer and Persoz, 1976; Mattauer et al., 1977; Brechbülher et al., 1988; Laville et al., 1991) while others argue that it is Cenozoic (Jacobshagen et al., 1988, Frizon de Lamotte et al., 2008). Nevertheless, no compressional structures of this kind appear in the red beds of the studied areas, except for localized foliation associated with strike-slip movements in the Tizi n'Test zone.

Furthermore, classical models of magnetic fabrics indicate that initially kmax axes cluster in a direction perpendicular to compression keeping kmin at the pole of bedding, while if compression continues kmin axes can show a girdled distribution.

In the 20 filtered sites, kmin axes are clustered with negligible scattering (Fig. 13a). This suggests that there is not a compressional record in these 20 red beds magnetic fabric sites. In addition to that, from the point of view of axes orientations, a possible compressional imprint in the direction of kmax axes can be discarded, since, opposite to magnetic fabrics in other sectors of the High Atlas (Moussaid et al., 2013), the orientation of the magnetic ellipsoid cannot be related to the Cenozoic shortening direction. In the same way, paleocurrent directions, which were analyzed in prior studies (Brown, 1980; Fabuel-Perez et al., 2009, and shown in Figs. 1c and d) do not seem to overlap with kmax axes orientation. At sample site observation scale (Fig. 4a, f), only in one site the orientation of the magnetic lineation is close to the paleocurrent direction, and precisely when this sedimentological marker overlaps the stretching direction inferred from tension gashes (site AG34). Therefore, a fluvial/alluvial origin for the clustering of the kmax axes is discarded for these 20 sites, that can be considered to record the extensional strain related to the tectonic setting in which the basin developed (Fig. 13b).

5.3. Late Triassic "Atlantic" versus "Atlasic" rifting in Western High Atlas

The 20 sites in which extensional fabrics can be interpreted are located in Upper Triassic units from Argana and Asni areas, showing an averaged WNW-ESE to NW-SE extension direction. nevertheless, the average orientation of kmax axes is different in the two areas: AG (N105E), AN southern sector (N150E) and AN northern sector (N130E). The relationship between magnetic lineation averages and surrounding structures is also different: in AG, kmax axes are perpendicular to NNE-SSW normal faults dominant in the offshore and onshore sectors of the Essaouira basin (Hafid 2000; Le Roy and Piqué, 2001; Mehdi et al., 2004), and oblique to inverted faults having overall Atlasic (E-W to NE-SW) orientation within the Argana Basin. In AN, the main faults strike NE-SW and probably correspond to inverted normal faults of Triassic age (Domènech et al., 2015), and kmax axes are approximately perpendicular to these faults, particularly in its southern sector.

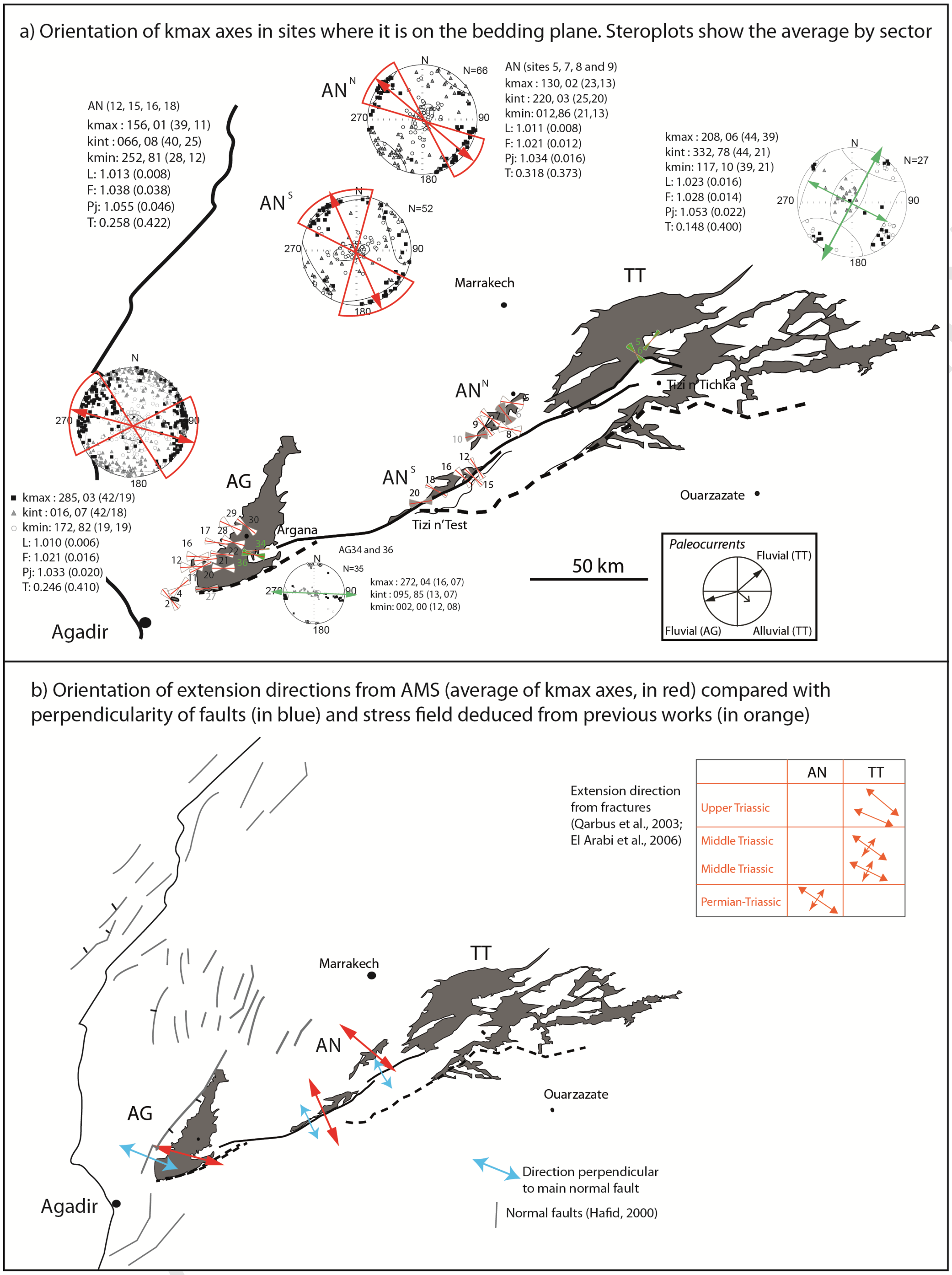

Fig. 13.

The extension directions inferred from magnetic fabrics suggest a strong influence of the "Atlantic" (WNW-ESE) extension in Argana Basin, which would be therefore controlled by the western rifted margin of Africa during the Triassic, versus an "Atlasic" extension, that would show minimum horizontal stress axes perpendicular to the normal faults within the chain, and in general to the E-W to ENE-WSW trend of the Atlasic basin. The prevalence of "Atlantic" extension is corroborated by the close directional relationship between the main normal faults in the Essaouira basin (Hafid, 2000; Le Roy and Piqué, 2001) and the extension directions found in this work by means of magnetic fabrics, contrasting with their obliquity with respect to Triassic onshore faults (some of them re-activated during the Atlasic compression) in the Argana Basin. Since the main signal corresponds to a WNW-ESE extension, movement along faults having Atlasic orientation in the Argana Basin (WSW-ESE to E-W) should have an oblique component, explaining transtensional movements on these faults. This also indicates that processes occurring in the future plate boundary (or rift axis) strongly influenced extension in the African mainland, imposing oblique movements on basement faults whose orientation was probably inherited from the Late-Variscan evolution. Changing extension directions inland (northern sector of AN area) also point to a decreasing influence of Atlantic extension towards the continent, being substituted by the stronger control on the extension direction exerted by pre-existing faults cutting across the basement and perpendicular to the axis of the Atlasic rift.

5.4 Mineralizations and basin evolution

The results obtained in this work also point to a significant importance of mineralizations occurring during the diagenetic evolution of Triassic rocks, able to switch axes of the primary magnetic ellipsoid. The source of fluids and metals as well as the age of mineralization in the Atlas remains controversial. Recent studies in Assif El Mal quartz–carbonate Zn–Pb (Cu-Ba-Fe-S) vein district seem to relate their origin to the Jurassic Atlantic rift and the associated hydrothermal activity involving regional low- to moderate-temperature fluids derived from evaporated seawater brines and organic water. The minimum temperature of entrapment of fluid inclusions at Assif El Mal ranges from 74°C to 198°C with a mode at 150°C to 160°C. Paleozoic rocks host the mineralizations in the Western High Atlas (Bouabdellah, 1988; Bouabdellah et al., 2009). Other Zn-Pb deposits are hosted in Bajocian limestones (Imilchil area, Mouguina and Daoudi, 2008). These areas are located to the NE of the AN, AS and TT areas.

These widespread mineralizations must be also explained within the frame of basin evolution. Conversely to the Atlantic-derived extension during basin formation and sedimentation, they seem more related to the development of the Atlas basins as an intraplate rift system, with a somewhat independent evolution from the rifted, oceanic growth and subsequently developed passive margin in its western flank. There are two interpretations for the Atlasic trough: The first one considers a rifting process that began during the Upper Triassic and lasted until the Bathonian or the Cretaceous. The second interpretation distinguishes two crustal-scale extensional events: (i) an initial event, beginning in Carnian time and leading to the development of a Late Triassic Atlasic true rift, (ii) a second event, starting early in the Toarcian, and responsible for a renewed crustal extension that disrupted the Liassic carbonate platform and led to the development of the fault-bounded Middle and High Atlas troughs.

The second interpretation agrees with widespread mineralizations during Jurassic times, related to hydrothermal events. Laville et al. (2004) suggest that after the Late Triassic, "true" Atlasic rift, thermal subsidence and lithospheric stretching occurred. Then, the first major marine incursion from the Tethys happened (~200 Ma) flooding the rifting area. During the Toarcian, fragmentation of the carbonate platform (transcurrent faulting) between Tizi n'Test and Gibraltar, favored the formation of rhomb-shaped basins (Middle and High Atlas troughs) limited by E-W and NE-SW faults that could favor circulation of fluids from deep sources.

6. Conclusions

Magnetic fabrics in red beds from the western High Atlas reveal a primary fabric (with kmin axes normal to bedding) in 28 sites out of 48 . This primary fabric can be related to extension in 20 sites out of these 28, with a reasonable clustering of kmax axes on the bedding plane. Secondary processes related to mineralization fluids provoked the new formation of hematite platelets and are responsible for axes switching and modification of the initial, primary fabric, maintaining the orientation (but not the relative magnitude) of the three axes of the magnetic ellipsoid.

The orientation of the primary fabric reveals the main extensional direction contemporary with sedimentation or early diagenesis in two of the three studied areas, indicating extension directions forming an angle of more than 25º between the western and eastern sectors. Results in the Argana area are indicative of the prevalence of Atlantic extension, while inland the main extension direction is perpendicular to the main Atlasic faults following the basin axis. According to the direction of the extension axes in the Argana area, a sinistral transtension can be interpreted in faults with Atlasic orientation.

Acknowledgements

Financial support comes from the National Spanish Research Program (Spanish Ministry of Economy and Competitiveness, MINECO), Project reference numbers: CGL2009-10840, CGL2009-08969, CGL2012-38481 and CGL2013-42670-P. Authors would like to acknowledge the use of Servicio General de Apoyo a la Investigación-SAI, Universidad de Zaragoza, and especially for the technical assistance of Cristina Gallego with the FESEM analyses.

Table 1. Location of sampled sites

		Latitude N	Longitude W	So Dip Direction	Dip
1	AG2	30º 30.269'	9º 26.314'	227	125
2	AG3	30º 30.692'	9º 26.062'	24	35
3	AG4	30º 30.692'	9º 26.062'	27	37
4	AG8	30º 36.394'	9º 20. 930'	295	38
5	AG11	30º 37.532'	9º 22.352'	184	42
6	AG12	30º 37.662'	9º 22.507'	5	36
7	AG16	30º 38.755'	9º 23.851'	250	6
8	AG17	30º 44.574'	9º 17.265'	11	39

9	AG20	30º 37.980'	9º 19.883'	26	20
10	AG21	30º 38.551'	9º 17.084'	326	33
11	AG22	30º 40.244'	9º 12.164'	270	71
12	AG23	30º 44.377'	9º 12.257'	95	47
13	AG24	30º 39.8	9º 14.093	352	34
14	AG25	30º 39.178'	9º 10.703'	332	22
15	AG26	30º 33.51'	9º 16.693'	240	72
16	AG27	30º 32.503'	9º 20.48'	230	40
17	AG28	30º 43.716'	9º 11.368'	354	48
18	AG29	30º 45.688'	9º 7.630'	215	20
19	AG30	30º 45.380'	9º 7.389'	333	21
20	AG31	30º 44.836'	9º 7.257'	180	35
21	AG32	30º 44.759'	9º 7.226'	320	26
22	AG33	30º 44.854'	9º 6.848'	321	37
23	AG34	30º 43.63'	9º 6.479'	300	18
24	AG35	30º 41.248'	9º 5.988'	33	31
25	AG36	30º 41.626'	9º 6.025'	146	30
26	AG37	30º 50.983'	8º 59.77'	305	35
27	TT1	31º 10' 48.5''	7º 27' 37''	70	15
28	TT3	31º 16' 07.9''	7º 24' 39.8''	195	60
29	TT4	31º 32' 19''	7º 30' 39.9''	220	40
30	TT5	31º 28' 20.5''	7º 24' 28.8''	342	32
31	TT6	31º 27' 6.8''	7º 23' 41.4''	65	22
32	TT7	31º 26' 9.7''	7º 24' 26.6''	344	100
33	AN1	31º 19' 0.72''	7º 57' 22.1''	130	22
34	AN4	31º 18' 45.4''	7º 57' 40.5''	158	33
35	AN5	31º 15' 57.7''	7º 58' 20.9''	284	48
36	AN6	31º 14' 32.4''	8º 0' 12.6''	330	30
37	AN7	31º 10' 41.8''	8º 4' 2.5''	25	37
38	AN8	31º 10' 26.4''	8º 3' 1.9''	1	11
39	AN9	31º 10' 18.8''	8º 5' 15''	1	73
40	AN10	31º 7' 7.2''	8º 7' 30.3''	315	75
41	AN12	31º 0' 11.2''	8º 9' 13.8''	200	45
42	AN14	30º 59' 15.5''	8º 9' 2.5''	32	60
43	AN15	30º 59' 26.1''	8º 9' 7.5''	5	42
44	AN16	30º 59' 11.5''	8º 12' 27.8''	124	14
45	AN17	30º 59' 6''	8º 13' 46.3''	161	45
46	AN18	30º 55' 34.4''	8º 16' 30.33''	153	43
47	AN19	30º 55' 0.3''	8º 17' 42.6''	45	30
48	AN20	30º 54' 25.5''	8º 19' 8.6''	25	30

FIGURE CAPTIONS

Fig. 1. a). Location of the Atlas Mountains in Western North Africa (from GeoMapApp, http://www.geomapapp.org). The Western Meseta is also known as Central or Moroccan Meseta. In red, outcrops of Permo-Triassic rocks. Names of the sampling areas are also written. b). Stratigraphy of the Permo-Triassic in Argana (West) and Tizi n'Tichka (East) areas. Redrawn from Hafid (2000), Baudon et al. (2012) and El Arabi et al. (2006). Notice the different scales. Co: conglomerates, S: sandstones.1c). Paleocurrents in the Argana area from Brown (1980). 1d) Stereoplot representing the summary of the main paleocurrent from previous works (Brown, 1980; Fabuel-Perez et al., 2009)

Fig. 2a) Geological map and location of the sampled sites in the three areas Argana: AG, Asni: AN and Tizi n'Tichka: TT. 2b) Poles to bedding.

Fig. 3. Field pictures of red beds in the Argana area. a) Panoramic view of Permian and Triassic units from AG33. b) N-dipping Triassic strata cut by conjugate fractures in AG21. c) Buttressing of steeply-dipping Triassic strata (on the left) against a partially reactivated normal fault in AG22. d) Dense fracture pattern in E-W striking, north-dipping beds in AG28. e) South-verging anticline associated with a re-activated normal fault in AG31. f) Small-scale buttressing against a South-dipping normal fault (originally dipping to the North, before folding) in AG32. Fractures appear as dashed white lines.

Fig. 4. Field pictures of selected sites where fractures and paleocurrent orientation data have been measured. a) Site AG23: Planar cross-bedding in sandstones. b) Site AG30: To the left of the picture, Riedel fractures (nearly perpendicular to bedding) associated with the displacement (hangingwall to the righ) of a normal fault zone. The north-dipping beds in the hangingwall (to the right) are intensely fractured, with closer spacing in the thinner beds (upper part of the sandstone sequence) and wider in the thicker beds (lower part). c) Site AG29a: Intensely fractured zone associated with normal faulting. d) Site AG29b: Normal faults and associated fractures in sandstone and shale layers. Note the change in thickness of the dark layer associated with the movement of the fault on the left. e) Site AG24: Extensional duplex associated with a NE-striking normal fault in alternating sandstones and lutites. The horse of sandstones is intensely fractured and cut across by numerous high-angle normal faults. f) Site AG34. Horizontal lamination (upper bed) and planar cross-bedding (lower beds) in sandstones. g) Site AG27: Small-scale normal fault of probable syn-sedimentary origin (note the change in thickness of the coarser-grained bed) in sub-horizontal

layers. h) Site AG25: Outcrop-scale horst limited by opposite-dipping, conjugate (after bedding is restored to the horizontal) normal faults in shallow-dipping beds.
Lower hemisphere, equal area stereoplots representing fractures (when possible, type of fracture is indicated). In situ projection for nearly horizontal bedding sites, or otherwise indicated next to the stereoplot. Black (grey) thick arrows represent the inferred main extension (or compression) directions. Cross-bedding and thin arrows indicating paleocurrent direction (after bedding correction to horizontal) also represented in 3 sites.

Fig. 5 a) Pj – T diagram. b) Pj versus Km diagram. c) Inclination of the magnetic ellipsoid axes once bedding is corrected to horizontal. Blue bars are type ii) sites, green bars are type iii) sites and grey names indicate type iv) sites, see text for more detail. To the right, the relative position of axes in a typical sedimentary fabric (kmin perpendicular to bedding, kmax and kint axes contained on the bedding plane).

Fig. 6. a) Types of magnetic fabrics regarding the inclination of the magnetic ellipsoid axes. b) Types of magnetic fabrics regarding the clustering of the magnetic axes. Stereoplots in paleogeographic coordinate system, lower hemisphere and equal area projection. Bedding is restored to horizontal.

Fig. 7. a) Comparison between RT and LT magnetic susceptibility values for analyzed samples. The slope of 1.5 and perfect paramagnetic (3.8) are also plotted for reference. b and c) Scalar values of the magnetic ellipsoids (Pj, T and Km) at room and low temperatures for comparison. Standard deviations are also represented.

Fig 8. RT (black) and LT (blue) stereoplots of the axes of the magnetic susceptibility ellipsoid. Lower hemisphere, equal area projection. Bedding is restored to horizontal.

Fig. 9. Thermomagnetic curves of selected samples. a) and b) Red: heating, blue: cooling. c) Blue: IRM acquisition curve, red: back-field. d) Thermal demagnetization of three IRM axes (green: 2 T, red: 0.4 T and blue: 0.12 T) of standard size paleomagnetic samples.

Fig. 10. SEM images and minerals identified after EDX qualitative analyses on thin sections. a) and c) show the general features of the two samples. b) and d) show particular characteristics such as the presence of barite in AG24 and iron-oxide and phyllosilictes in AG30. e) Post-sedimentary hexagonal and flat iron oxides forming a ball and surrounding phyllosilicates (typical habit of hematite). The stereoplots (lower hemisphere, equal area projection) show the orientation of the

magnetic axes of the two selected samples at RT (black) and LT (blue). Sketches inspired in f) AG30 and g) AG24, parallel to bedding, showing the primary and secondary fabrics and the different orientations of the magnetic axes with respect to bedding. Blue represents iron-oxides, grey phyllosilicates and white quartz minerals. Scale is approximate.

Fig. 11. Stereoplots of principal magnetic axes of type ii), iii) and iv) fabrics.

Fig 12. Average kmax axes orientation and their confidence angle errors. Only sites with kmax horizontal once bedding is restored are represented. In white, type i), in green, type ii).

Fig. 13. A) Average of the 20 selected sites of type i) and type ii), in three sectors. B) Comparison of extension direction inferred from AMS data (red arrows) with extension directions compiled from previous studies in orange (El Arabi et al., 2003; Qarbous et al., 2003 and references therein) and the orientation perpendicular to normal faults (in blue in AG and in black in AN, Hadif, 2000).

REFERENCES

Aït Brahim, L. Ait, and Abdelfatah Tahiri. 1996. Rotation horaire des contraintes et mécanismes d'ouverture et de fermeture des bassins permiens du Maroc central. Le Permien et le Trias du Maroc, état des connaissances, PUMAG, Marrakech, Maroc, 87-98.

Anderson, E.M. 1951. The dynamics of faulting. Oliver and Boyd, Edinburg, 206 p.

Arboleya M.L., Teixell A., Charroud M., Julivert M. 2004. A structural transect through the High and Middle Atlas of Morocco, J. Afr. Earth Sci. 39, 319–327.

Aubourg, C., Robion, P. 2002. Composite ferromagnetic fabrics (magnetite, greigite) measured by AMS and partial AARM in weakly strained sandstones from western Makran, Iran. Geophys. J. Int. (2002) 151 (3): 729-737. doi: 10.1046/j.1365-246X.2002.01800.x

Aubourg, C., Rochette, P., Stéphanc, J.-F., Popoff, M., Chabert-Pellinec, C., 1999. The magnetic fabric of weakly deformed Late Jurassic shales from the southern subalpines chains (French Alps): evidence for SW-directed tectonic transport direction. Tectonophysics 307 (1–2), 15–31.

Averbuch, O., Frizon de Lamotte, D., Kissel, C., 1992. Magnetic fabric as a structural indicator of the deformation path within a fold-thrust structure: a test case from the Corbières (NE Pyrenees, France). J. Struct. Geol. 14, 461–474.

Bando, Y., Kiyama, M. Yamamoto, N. Takada, T., Shinjo, *T.*, Takaki, H. 1965. Magnetic properties of -Fe_2O_3 fine particles, J. Phys. Soc. Jpn., 20, 2086.

Baudon, C., Redfern, J., Van Den Driessche, J. 2012. Permo-Triassic structural evolution of the Argana Valley, impact of the Atlantic rifting in the High Atlas, Morocco. Journal of African Earth Sciences, 65, 91-104.

Beauchamp W., Barazangi M., Demnati A., El Alji M. 1996. Intracontinental rifting and inversion: Missour Basin and Atlas Mountains, Morocco, AAPG Bull. 80, 1459–1482.

Biron, P.E., 1982. Le Permo-Trias de la région de l'Ourika (Haut Atlas de Marrakech, Maroc), Sédimentologie tectonique et métallogénie, Thèse de 3ème cycle. Institut Dolomieu, Grenoble, 170 p

Biron, P.E., Courtinant, B. 1982. Contribution palynologique à la connaissance du Trias du Haut Atlas de Marrakech, Geobios, Lyon, 15, 231-235.

Borradaile, G.J., Henry, B. 1997. Tectonic applications of magnetic susceptibility and its anisotropy. Earth-Science Reviews, 42, 49-93.

Borradaile, G.J., Jackson, M., 2004. Anisotropy of magnetic susceptibility (AMS): magnetic petrofabrics of deformed rocks. In: Martín- Hernández, F., Lu•neburg, C.M., Aubourg, C., Jackson, M. (Eds.), Magnetic Fabrics: Methods and Applications. Geological Soc. Special Pub, vol. 238, 299-360

Borradaile, G.J., Tarling, D.H. 1981. The influence of deformation mechanisms on magnetic fabrics weakly deformed rocks. Tectonophysics, 77, 151-168.

Bouchez J. L. 1997. Granite is never isotropic: an introduction to AMS studies of granitic rocks, in: Bouchez J. L., Hutton D. H. W., Stephen W. E. (Eds), Granite: from segregation of melt to emplacement fabrics, Kluwer Acad. Pub., 95-112.

Bouabdellah, M. (1988). Etude pétrographique et métallogénique du district polymétallique à Pb-Zn-Cu-Ba-Fe-Sn d'Assif El Mal-Bouzouga, Haut Atlas de Marrakech, Maroc. Unpubl Ph. D (Doctoral dissertation, Thesis, University of Marrakech).

Bouabdellah, M., Beaudoin, G., Leach, D. L., Grandia, F., Cardellach, E. (2009). Genesis of the Assif El Mal Zn–Pb (Cu, Ag) vein deposit. An extension-related Mesozoic vein system in the High Atlas of Morocco. Structural, mineralogical, and geochemical evidence. *Mineralium Deposita*, *44*(6), 689-704.

Brechbülher, Y.A., Bernasconi, R., Schaer, J.P. 1988. Jurassic sediments of the Central High Atlas of Morocco: deposition burial and erosion history. In: V Jacobshagen (Ed.), The Atlas system of Morocco, Lecture Notes in Earth Sciences, vol. 15, Springer-Verlag, Berlin, 201–215

Brown R.H. 1980. Triassic rocks of Argana valley, southern Morocco, and their regional structural implications, A.A.P.G. Bull. 64, 988–1003.

Chadima, M., Hrouda, F., Melichar , R. 2006. Magnetic fabric study of the SE Rhenohercynian Zone (Bohemian Massif): Implications for dynamics of the Paleozoic accretionary prism. Tectonophysics, 418, 93-109.

Chadima, M., Hansen, A., Hirt, A.M., Hrouda, F., Siemes, H. 2004. Phyllosilicate preferred orientation as a control of magnetic fabric: evidence from neutron texture goniometry and low and high-field magnetic anisotropy (SE Rhenohercynian Zone of Bohemian Massif). In: Martín- Hernández, F., Lu•neburg, C.M., Aubourg, C., Jackson, M. (Eds.), Magnetic Fabrics: Methods and Applications. Geological Soc. Special Pub, vol. 238, 361-380

Chadima, M. and Hrouda, F. 2009. Cureval 8.0: Thermomagnetic Curve Browser for Windows. *Agico, Inc*.

Chadima, M. and Jelinek, V. 2009. Anisoft 4.2: Anisotropy Data Browser for Windows. *Agico, Inc*

Cifelli, F., Mattei, M., Hirt, A.M., Gunther, A., 2004. The origin of tectonic fabrics in "undeformed" clays: The early stages of deformation in extensional sedimentary basins. Geophys. Res. Lett. 31, L09604. doi:10.1029/2004GL019609.

Cifelli, F., Mattei, M., Chadima, M., Hirt, A.M., Hansen, A., 2005. The origin of the tectonic lineation in extensional basins: Combined neutron texture and magnetic analysis on "undeformed" clays. Earth Plan. Sci. Lett. 235, 62–78.

Cifelli, F., Rossetti, F., Mattei, M., 2007. The architecture of brittle postorogenic extension: results from an integrated structural and paleomagnetic study in north Calabria (southern Italy). Geol. Soc. Am. Bull. 119 (1/2), 221–239.

Cogné, J.P., Gapais, D. 1986. Passive rotation of hematite during deformation: a comparison of simulated and natural redbeds fabrics. Tectonophysics, 121, 365-372.

Cogné, J.P., Perroud, H. 1985. Strain removal applied to paleomagnetic directions in an orogenic belt: the Permian red slates of the Alpes Maritimes, France. Earth and Planetary Science Letters, 72, 125-140

Collinson, D. W. 1983. Methods in palaeomagnetism and rock magnetism.

Dankers, P. H. M. 1978. Magnetic properties of dispersed natural iron-oxides of known grain size.

Daly, L., Zinsser, H. 1973. Étude comparative des anisotropies magnétiques superposées et leur séparation. Comptes rendus hebdomadaires des séances de l'Académie des Sciences (Paris), Série B, 264, 1377-1380.

Debacker, T.N., Robion, Ph., Sintubin, M., 2004. The anisotropy of magnetic susceptibility (AMS) in low-grade, cleaved pelitic rocks: influence of cleavage/bedding angle and type and relative orientation of magnetic carriers. In: Martín- Hernández, F., Lu•neburg, C.M., Aubourg, C., Jackson, M. (Eds.), Magnetic Fabrics: Methods and Applications. Geological Soc. Special Pub, vol. 238, pp. 77-107.

Debacker, T.N., Hirt, A., Sintubin, M., Robion, Ph. 2009. Differences between magnetic and mineral fabrics in low-grade, cleaved siliciclastic pelites: A case study from the Anglo-Brabant Deformation Belt (Belgium) Tectonophysics, 466, 32–46

De Boer, C. B., Dekkers, M. J. 2001. Unusual thermomagnetic behaviour of hematites: neoformation of a highly magnetic spinel phase on heating in air. Geophysical Journal International, 144(2), 481-494.

Domènech, M., Teixell, A., Babault, J., Arboleya, M.L. 2015. The inverted Triassic rift of the Marrakech High Atlas: A reappraisal of basin geometries and faulting histories, Tectonophysics (2015), In press. http://dx.doi.org/10.1016/j.tecto.2015.03.017

El Arabi, E.H., Ferrandini, J., Essamoud, R., 2003. Triassic stratigraphy and structural evolution of a rift basin: the Ec Cour basin, High atlas of Marrakech, Morocco. Journal of African Earth Sciences 36 (1–2), 29–39.

El Arabi E.H., Diez J.B., Broutin J., Essamoud R. 2006. Première caractérisation palynologique du Trias moyen dans le Haut Atlas; implications pour l'initiation du rifting téthysien au Maroc, C. R. Geoscience 338, 641–649.

El Wartiti, M., F. Medina, and D. Fadli. 1992. Effects of Central Atlantic early rifting in the northern border of the Berrechid–El Gara Basin (Morocco). Gaia 4, 31-38.

Fabuel-Perez, I., Redfern, J., Hodgetts, D., 2009. Sedimentology of an intra-montane rift-controlled fluvial dominated succession: the upper Triassic Oukaimeden sandstone formation, Central High Atlas, Morocco. Sedimentary Geology 218 (1–4), 103–140.

Flanders, P. J., Remeika, J. P. 1965. Magnetic properties of hematite single crystals. Philosophical Magazine, 11(114), 1271-1288.

Fiechtner, L., Friedrichsen, H., Hammerschmidt, K., 1992. Geochemistry and geochronology of Early Mesozoic tholeiites from Central Morocco. Geologische Rundschau 81, 45–62.

Frizon de Lamotte, D., Saint Bézar B., Bracène R., Mercier E., 2000. The two main steps of the Atlas building and geodynamics of the western Mediterranean, Tectonics 19 , 740–761.

Frizon de Lamotte, D., M. Zizi, Y. Missenard, M. Hafid, M. El Azzouzi, R. C. Maury, A. Charrière, Z. Aki, M. Benammi, and A. Michard (2008), The Atlas system, in Continental Evolution: The Geology of Morocco, Lect. Notes Earth Sci. Ser., vol. 116, edited by A. Michard, O. Saddiqi, and A. Chalouan, pp. 133–202, doi:10.1007/978-3-540-77076-3_4, Springer, Berlin.

Fuller, M. 1963. Magnetic anisotropy and paleomagnetism. Journal of Geophysical Research, 68, 293-309.

García-Lasanta, C., Oliva-Urcia, B., Román-Berdiel, T., Casas, A. M., Pérez-Lorente, F. 2013. Development of magnetic fabric in sedimentary rocks: insights from early compactional structures. Geophysical Journal International, ggt098.

García-Lasanta, C., Oliva-Urcia, B., Román-Berdiel, T., Casas, A.M., Hirt, A.M. 2014. Understanding the Mesozoic kinematic evolution in the Cameros basin (Iberian Range, NE Spain) from magnetic subfabrics and mesostructures. Journal of Structural Geology 66, 84-101

Graham, J.W. 1954. Magnetic susceptibility anisotropy, an unexploited petrofabric element. Geological Society of America Bulletin, 65, 1257-1258.

Guerrero-Suárez, S., Martín-Hernández, F. 2012. Magnetic anisotropy of hematite natural crystals: increasing low-field strength experiments, International Journal of Earth Sciences, 101. 625-636

Guilbert, J.M., Park C.F. 1986. The Geology of Ore Deposits, Freeman, New York

Hafid M. 2000. Triassic–Early Liassic extensional systems and their Tertiary inversion, Essaouira Basin (Morocco). Marine Petrol. Geol. 17, 409–429.

Hafid M. 2006. Styles structuraux du Haut Atlas de Cap Tafelney et de la partie septentrionale du Haut Atlas occidental: tectonique salifère et relation entre l'Atlas et l'Atlantique. Notes Mém. Serv. Géol. Maroc 465, 172 pp.

Hafid, M., Zizi, M., Bally, A.W., Ait Salem, A. 2006. Structural styles of the western onshore and offshore termination of the High Atlas, Morocco. C. R. Geosci., 338, 50–64

Hancock, P. (1985). Brittle microtectonics: principles and practice. Journal of Structural Geology, 7, 437-457

Hilley, G.E., Arrowsmith, J.R., Amoroso, L. (2001). Interaction between normal faults and fractures and fault scarp morphology. Geophysical Research Letters, 28 (19), 3777-3780

Hirt, A., Lowrie, W., Lünenburg, C., Lebit, H., Engelder T. 2004. Magnetic fabric development in the Ordovician Martinsburg Formation, Pennsylvania. In: F. Martín-Hernandez, C.M. Lünenburg, C. Aubourg, M. Jackson (Eds.), Magnetic Fabrics, Geological Society of London Special Publication, vol. 238 (2004), pp. 109–126

Hoepffner, C., Soulaimani, A., Piqué ,A. 2005. The Moroccan Hercynides. J. Afr. Earth Sci., 43, 144–165

Hofmann, A., Tourani, A., Gaupp, R., 2000. Cyclicity of Triassic to Lower Jurassic continental red beds of the Argana Valley, Morocco: implications for palaeoclimate and basin evolution. Palaeogeography, Palaeoclimatology, Palaeoecology 161 (1–2), 229–266.

Housen, B.A. van der Pluijm, B.A. 1990. Chlorite control of correlations between strain and anisotropy of magnetic susceptibility. Physics of the Earth and Planetary Interiors, 61, 315–323

Housen, B.A. van der Pluijm••B.A. 1991. Slaty cleavage development and magnetic anisotropy fabrics. Journal of Geophysical Research, 96, 9937–9946

Housen, B.A., Richter, C., van der Pluijm, B.A., 1993. Composite magnetic anisotropy fabrics: experiments, numerical models, and implications for the quantification of rock fabrics. Tectonophysics, 220, 1–12.

Hrouda, F. 1980. Magnetocrystalline anisotropy of rocks and massive ores: A mathematical model study and its fabric implications. Journal of Structural Geology, 2, 459–462

Huon, S., Cornée, J.J., Piqué, A., Rais, N., Clauer, N., Liewig, N., Zayane, R. 1993. Mise en évidence au Maroc d'événements thermiques d'âge triasico-liasique liés à l'ouverture de l'Atlantique. Bulletin de la Société géologique de France, 164, 165–176

Izquierdo-Llavall, E., Casas-Sainz, A.M., Oliva-Urcia, B. 2013. Heterogeneous deformation recorded by magnetic fabrics in the Pyrenean Axial Zone Journal of Structural Geology, 57, 97–113

Jabour H., Dakki M., Nahim M., Charrat F., El Alji M., Hssain M., Oumalch F., El Abibi R. 2004. The Jurassic depositional system of Morocco and play concept, MAPG Mem. 1, 5–39.

Jacobshagen V., Brede R., Hauptmann M., Heinitz W., Zylka R. 1988. Structure and post-Paleozoic evolution of the Central High Atlas, in Jacobshagen V. (Ed.), The Atlas system of Morocco, Lect. Notes Earth Sci. 15, 245–271.

Jelinek, V. 1981. Characterization of the magnetic fabric of rocks. Tectonophysics, 79(3), T63-T67.

Jiang, Z., Liu, Q., Dekkers, M. J., Colombo, C., Yu, Y., Barrón, V., Torrent, J. 2014. Ferro and antiferromagnetism of ultrafine-grained hematite. Geochemistry, Geophysics, Geosystems, 15(6), 2699-2712.

Kündig, W., Bommel, H., Constabaris, G., Lindquist, R. H. 1966. Some properties of supported small a-Fe203 particles determined with the Mössbauer effect: Phys. Rev. 142, 327-333.

Laville E., Petit J.P. 1984. Role of synsedimentary strike-slip faults in the formation of the Moroccan Triassic basins, Geology 12, 424–427.

Laville E., Piqué A. 1991. La distension crustale atlantique et atlasique au Maroc au début du Mésozoïque: le rejeu des structures hercyniennes, Bull. Soc. géol. Fr. 162, 1161–1171.

Laville E., Piqué A. 1992. Jurassic penetrative deformation and Cenozoic uplift in the central High Atlas (Morocco): A tectonic model. Structural and orogenic inversions, Geol. Rundsch. 81, 157–170.

Laville E., Lesage J.L., Séguret M. 1977. Géométrie, cinématique, dynamique de la tectonique atlasique sur le versant sud du Haut Atlas marocain : aperçu sur les tectoniques hercyniennes et tardihercyniennes, Bull. Soc. géol. Fr. (7) 19, 527–539.

Laville E, Fedan, B., Piqué, A. 1991. Déformation synschisteuse jurassique, orogenèse cénozoï•que: deux étapes de la structuration du Haut Atlas (Maroc) Comptes rendus de l'Académie des Sciences de Paris, 312 (II),1205–1211

Laville, E., A. Piqué, M. Amhar, and M. Charroud, 2004. A restatement of the Mesoizoic Atlasic Rifting (Morocco), J. Afr. Earth Sci., 38, 145–153, doi:10.1016/j.jafrearsci.2003.12.003.

Leonhardt, R. 2006. RockMagAnalyzer 1.0

Le Roy, P., Piqué, A. 2001) Triassic–Liassic Western Moroccan synrift basins in relation to the Central Atlantic opening. *Marine Geology*, *172*(3), 359-381.

Lowrie, W. 1990. Identification of ferromagnetic minerals in a rock by coercivity and unblocking temperature properties. *Geophysical Research Letters*, *17*(2), 159-162.

Lüneburg, C. M., Lampert, S. A., Lebit, H. D., Hirt, A. M., Casey, M., Lowrie, W. 1999. Magnetic anisotropy, rock fabrics and finite strain in deformed sediments of SW Sardinia (Italy). Tectonophysics, 307(1), 51-74.

Mader, N.K., Redfern, J. 2011. A sedimentological model for the continental Upper Triassic Tadrart Ouadou Sandstone Member: recording an interplay of climate and tectonics (Argana Valley; South-west Morocco). Sedimentology 58 (5), 1247–1282.

Mamtani, M. A., Sengupta, P. 2010. Significance of AMS analysis in evaluating superposed folds in quartzites. Geological Magazine, 147, 910–918.

Martín-Hernández, F., Guerrero-Suárez, S. 2012. Magnetic anisotropy of hematite natural crystals: high field experiments. International Journal of Earth Sciences 101, 637-647.

Márton, E., Márton, P., Heller, F. 1980. Remanent magnetization of a Pliensbachian limestone sequence at Bakonycsernye (Hungary). Earth and Planetary Science Letters, 48(1), 218-226.

Mattauer, M., Tapponier P., Proust F. 1977. Sur les mécanismes de formation des chaînes intracontinentales. L'exemple des chaînes atlasiques du Maroc., Bull. Soc. géol. Fr. (7) 19, 521–526.

Mattei, M., Sagnotti, L., Faccenna, C., Funiciello, R., 1997. Magnetic fabric of weakly deformed clay-rich sediments in the Italian peninsula: relationship with compressional and extensional tectonics. Tectonophysics 271, 107-122.

Mattei, M., Speranza, F., Argentieri, A., Rosseti, F., Sagnotti, L., Funiciello, R., 1999. Extensional tectonics in the Amantea basin (Calabria, Italy): a comparison between structural and magnetic anisotropy data. Tectonophysics 307, 33-49.

McCabe, C., Jackson, M., Ellwood, B.B., 1985. Magnetic anisotropy in the Trenton limestone: results of a new technique, anisotropy of anhysteretic susceptibility. Geophys. Res. Lett. 12, 333–336.

Mehdi, K., Griboulard, R., Bobier, C. 2004. Rôle de l'halocinèse dans l'évolution du bassin d'Essaouira (Sud-Ouest marocain). Comptes Rendus Géoscience, 336(6), 587-595.

Medina, F., 1991. Superimposed extensional tectonics in the Argana Triassic formations (Morocco), related to the early rifting of the central Atlantic. Geological Magazine 128 (5), 525–536.

Medina, F. 2000. Structural styles of the Moroccan Triassic basins. Zbl. Geol. Paläont, 9-10.

Medina, F., A. Errami. 1996. L'inversion tectonique dans le bassin de Tine Mellil (Haut Atlas occidental, Maroc), Implications sur le fonctionnement de la faille de Tizi n'Test. Gaia 12, 9-18.

Medina F., Vachard D., Colin J.P., Ouarhache D., Ahmamou M. 2001. Charophytes et ostracodes du niveau carbonat´e de Taourirt Imzilen (Membre d'Aglegal, Trias d'Argana); implications stratigraphiques. Bull. Inst. Sci. Rabat 23, 21–26.

Michard, A., Frizon de Lamotte, D., Liégeois J.P., Saddiqi, O., Chalouan, A. 2008. Continental Evolution: The Geology of Morocco. Lecture Notes 395 in Earth Sciences 116, Springer-Verlag Berlin Heidelberg

Morin, F. J. 1950. Magnetic susceptibility of a-Fe2O3 and a-Fe2O3 with added titanium, Phys. Rev., 78, 819–820, doi:10.1103/PhysRev.78.819.2.

Morrish A.H. 1994. Canted antiferromagnetism: hematite. World Scientific Publishing C. Pte Ltd, Singapore

Mouguina, E. M., Daoudi, L. 2008. Pb-Zn mineralization of the Ali ou Daoud area (Central High Atlas, Morocco): characterisation of the deposit and relationships with the clay assemblages.

Moussaid, B., El Ouardi, H., Casas-Sainz, A., Villalaín, J.J., •••á•••••••••••••••••••••••••••••••••••••• Torres-López, S. 2013. Magnetic fabrics in the Jurassic–Cretaceous continental basins of the northern part of the Central High Atlas (Morocco): Geodynamic implications. Journal of African Earth Sciences, 87, 13–32

Muzio, R., Scaglia, F., Masquelin, H. 2013. Titaniferous magnetite and barite from the San Gregorio de Polanco dike swarm, Paraná Magmatic Province, Uruguay. Earth Sciences Research Journal, 17(2), 151-158.

Oliva-Urcia, B., Larrasoaña, J. C., Pueyo, E. L., Gil, A., Mata, P., Parés, J. M. 2009. Disentangling magnetic subfabrics and their link to deformation processes in cleaved sedimentary rocks from the Internal Sierras (west central Pyrenees, Spain). Journal of Structural Geology, 31(2), 163-176.

Oliva-Urcia, B., Roman-Berdiel, T., Casas, A.M., Pueyo, E.L., Osácar, C. 2010. Tertiary compressional overprint on Aptian–Albian extensional magnetic fabrics, North-Pyrenean Zone. Journal of Structural Geology 32, 362-376.

Oliva-Urcia, B., Rahl, J.M., Schleicher, A.M., Parés J.M. 2010. Correlation between the anisotropy of the magnetic susceptibility, strain and X-ray Texture Goniometry in phyllites from Crete, Greece. Tectonophysics, 486, 120-131

Oliva-Urcia, B., Casas, A. M., Soto, R., Villalaín, J. J., Kodama, K. 2011. A transtensional basin model for the Organyà basin (central southern Pyrenees) based on magnetic fabric and brittle structures. Geophysical Journal International, 184(1), 111-130.

Oliva-Urcia, B., Casas, A.M., Ramón, M.J., Leiss, B., Mariani, E., Román-Berdiel, T. 2012. On the reliability of AMS in ilmenite-type granites: an insight from the Marimanha pluton, central Pyrenees. Geophys. J. Int. 189, 187–203

Oliva-Urcia, B., Román-Berdiel, T., Casas, A. M., Bogalo, M. F., Osácar, M. C., García-Lasanta, C. 2013. Transition from extensional to compressional magnetic fabrics in the Cretaceous Cabuérniga basin (North Spain). Journal of Structural Geology, 46, 220-234.

Olsen, P.E., Kent, D.V., Et-Touhami, M., Puffer, J.H., 2003. Cyclo-, magneto-, and biostratigraphic constraints on the duration of the CAMP event and its relationship to the Triassic–Jurassic boundary. In: Hames, W.E., McHone, J.G., Renne, P.R., Ruppel, C. (Eds.), The Central Atlantic Magmatic Province: Insights From Fragments of Pangea. Geophysical Monograph Series, vol. 136, pp. 7–32.

Özdemir, Ö., Dunlop, D. J., Berquo, T. S. 2008. Morin transition in hematite: Size dependence and thermal hysteresis. Geochemistry, Geophysics, Geosystems, 9(10).

Parés, J.M., van der Pluijm, B., Dinarès-Turell J. 1999. Evolution of magnetic fabrics during incipient deformation of mudrocks (Pyrenees, northern Spain). Tectonophysics, 307, 1–14

Petit, J.P. 1976. La zone de décrochements du Tzi n'Test (Maroc) et son fonctionnement depuis le carbonifère. Diss. Université des Sciences et Techniques du Languedoc.

Petit, J. P. 1987. Criteria for the sense of movement on fault surfaces in brittle rocks. *Journal of Structural Geology*, *9*(5), 597-608.

Petrovský, E., Kapi ka, A. 2006. On determination of the Curie point from thermomagnetic curves. Journal of Geophysical Research: Solid Earth (1978–2012), 111(B12).

Proust F., Petit J-P., Taponnier P. 1977. L'accident de Tizi n'Test et le rôle des décrochements dans la tectonique du Haut Atlas occidental (Maroc). Bull. Soc. géol. Fr., 7, XIX, 541-551.

Qarbous A., Medina F., Hoepffner C. 2003. Le bassin de Tizi n'Test (Haut Atlas, Maroc): Exemple d'évolution d'un segment oblique au rift de l'Atlantique central au Trias. Can. J. Earth Sci., 40, 949–964.

Qarbous, A., Hoepffner, C., Medina, F. 2009. Mise en évidence d'un niveau à méga-slumps au sommet de la série triasique du bassin de Tizi n'Test (Haut Atlas, Maroc). Bulletin de l'Institut Scientifique, Rabat, section Sciences de la Terre, 31, 35-39.

Ramsay, J.G., Huber, M.I. (1987). The techniques of modern structural geology. Volume 2: folds and fractures. Academic Press, London, 391 p.

Richter, C., van der Pluijm, B.A., Housen, B.A. 1993.The quantification of crystallographic preferred orientation using magnetic anisotropy. Journal of Structural Geology, 15, 113–116

Richter, C., van der Pluijm, B. A. 1994. Separation of paramagnetic and ferrimagnetic susceptibilities using low temperature magnetic susceptibilities and comparison with high field methods. Physics of the Earth and Planetary Interiors, 82(2), 113-123.

Rochette, P. 1987. Magnetic susceptibility of the rock matrix related to magnetic fabric studies, J. Struct. Geol., 9, 1015–1020.

Saint-Bézar, B., Hebert, R.L., Aubourg, C., Robion, P., Swennen, R., Frizon de Lamotte, D. 2002. Magnetic fabric and petrographic investigation of hematite-bearing sandstones within ramp-related folds: examples from the South Atlas front (Morocco). Journal of Structural geology, 24, 1507-1520.

Schaer, J.P. Persoz F. 1976. Aspects structuraux et pétrographiques du Haut Atlas calcaire de Midelt (Maroc). Bulletin de la Societé géologique de France (7), 18, 1239–1250

Stephenson, A. Sadikun, S., Potter, D.K. 1986. A theoretical and experimental comparison of the anisotropies of magnetic susceptibility and remanence in rocks and minerals. Geophysical Journal of the Royal Astronomical society, 84, 185-200.

Tarling, D.H., Hrouda, F. 1993. The Magnetic Anisotropy of Rocks. Chapman and Hall, London.

Teixell A., Arboleya M.-L., Julivert M., Charroud M. 2003. Tectonic shortening and topography of the central High Atlas (Morocco), Tectonics 22, 1051

Tourani, A., Lund, J.J., Benaouiss, N., Gaupp, R., 2000. Stratigraphy of Triassic syn-rift deposition in Western Morocco. Zentralblatt fuer Geologie und Palaeontologie 1 (9–10), 1193–1215.

Table 2. Average value of magnetic susceptibility (Km), standard magnetic lineation (L) foliation (F), corrected anisotropy degree (Pj) and shape parameter (T) of every site, with the corresponding standard deviation. Orientation of the magnetic ellipsoid axes (kmax, kint and kmin) and confidence angles when bedding is corrected to horizontal.

	average Km	stand. dev.	average L	stand. dev.	average F	stand. dev.	average Pj	stand. dev.	average T	stand. dev.	kmax dec	kmax inc	kmax conf. ang.	kint dec	kint inc
1	1.15E-04	3.17E-05	1.008	0.002	1.043	0.019	1.055	0.023	0.651	0.165	321	14	20/11	231	
2	6.87E-05	3.53E-06	1.004	0.004	1.005	0.006	1.009	0.008	-0.046	0.463	52	12	71/35	322	
3	8.98E-05	2.33E-05	1.008	0.005	1.031	0.024	1.042	0.027	0.456	0.328	51	0	22/8	321	
4	1.04E-04	1.50E-05	1.006	0.002	1.009	0.004	1.015	0.003	0.104	0.417	283	21	59/26	188	
5	6.01E-05	2.75E-05	1.004	0.003	1.013	0.011	1.019	0.013	0.426	0.287	87	4	28/6	357	
6	3.68E-04	5.45E-05	1.010	0.005	1.014	0.005	1.025	0.007	0.202	0.377	64	3	14/3	333	
7	1.07E-04	1.47E-05	1.006	0.001	1.016	0.006	1.023	0.007	0.385	0.22	93	3	27/4	3	
8	1.03E-04	8.94E-06	1.006	0.003	1.018	0.007	1.025	0.009	0.518	0.291	279	9	17/15	186	
9	8.27E-05	3.17E-05	1.008	0.004	1.026	0.012	1.036	0.015	0.473	0.286	84	6	26/11	353	
10	4.19E-05	2.00E-05	1.011	0.006	1.016	0.015	1.028	0.019	0.016	0.38	90	3	24/20	181	
11	9.25E-05	3.34E-05	1.014	0.004	1.035	0.019	1.051	0.023	0.326	0.364	95	3	14/4	185	
12	1.37E-04	5.22E-05	1.021	0.007	1.039	0.021	1.062	0.022	0.233	0.325	96	68	16/6	302	
13	8.99E-05	3.85E-05	1.01	0.006	1.005	0.002	1.016	0.006	-0.18	0.437	18	80	17/13	272	
14	2.84E-04	3.67E-05	1.048	0.026	1.151	0.029	1.217	0.035	0.514	0.227	308	79	18/4	88	
15	8.62E-05	2.45E-05	1.012	0.01	1.024	0.01	1.037	0.013	0.329	0.315	80	71	34/11	274	
16	1.06E-04	2.07E-05	1.016	0.003	1.007	0.004	1.023	0.004	-0.421	0.296	84	9	15/6	346	
17	4.96E-05	2.32E-05	1.008	0.006	1.009	0.005	1.018	0.008	-0.024	0.408	105	12	26/16	199	
18	1.53E-04	3.20E-05	1.019	0.006	1.034	0.019	1.055	0.019	0.222	0.323	294	4	32/20	25	
19	1.43E-04	3.52E-05	1.015	0.005	1.027	0.01	1.043	0.01	0.256	0.263	309	4	17/14	40	
20	1.76E-04	2.26E-05	1.017	0.005	1.016	0.009	1.033	0.008	-0.074	0.376	100	81	14/7	240	
21	1.17E-04	2.88E-05	1.007	0.003	1.008	0.003	1.015	0.003	0.067	0.372	268	2	53/12	166	
22	1.22E-04	1.96E-05	1.015	0.007	1.022	0.017	1.038	0.018	0.098	0.407	283	86	21/5	101	
23	2.47E-04	5.30E-05	1.013	0.007	1.099	0.038	1.125	0.044	0.736	0.157	102	19	19/2	283	
24	1.81E-04	3.05E-05	1.053	0.008	1.066	0.004	1.07	0.005	0.623	0.241	280	67	12/4	79	
25	5.43E-04	1.28E-04	1.077	0.01	1.04	0.016	1.123	0.015	-0.323	0.195	263	6	4/3	112	
26	2.65E-04	1.11E-04	1.012	0.019	1.013	0.02	1.026	0.041	-0.011	0.364	145	1	51/6	51	
27	1.32E-04	7.25E-05	1.005	0.002	1.017	0.006	1.023	0.008	0.505	0.156	267	3	66/18	176	
28	2.18E-04	2.98E-05	1.014	0.006	1.015	0.006	1.03	0.009	0.03	0.255	108	82	19/15	13	
29	6.80E-05	1.27E-05	1.006	0.009	1.012	0.02	1.019	0.028	0.095	0.5	148	5	50/24	30	
30	3.27E-04	6.58E-05	1.037	0.007	1.029	0.013	1.069	0.014	-0.15	0.227	219	2	11/6	319	
31	2.25E-04	3.36E-05	1.009	0.005	1.027	0.016	1.038	0.017	0.424	0.318	139	17	18/9	317	
32	1.32E-04	1.92E-05	1.006	0.002	1.016	0.005	1.023	0.004	0.442	0.29	47	5	47/17	315	
33	1.33E-04	2.86E-05	1.005	0.002	1.015	0.009	1.021	0.009	0.357	0.467	312	8	39/17	43	
34	4.62E-05	1.65E-05	1.005	0.003	1.006	0.003	1.011	0.004	0.041	0.49	16	23	82/34	280	
35	1.18E-04	5.30E-05	1.004	0.003	1.007	0.005	1.011	0.004	0.246	0.51	98	5	31/14	188	
36	1.06E-04	1.73E-05	1.004	0.002	1.007	0.002	1.007	0.002	0.046	0.402	145	7	34/34	47	
37	1.78E-04	2.76E-05	1.009	0.003	1.026	0.011	1.037	0.012	0.425	0.256	306	3	20/11	216	
38	1.43E-04	3.42E-05	1.008	0.003	1.03	0.004	1.04	0.006	0.592	0.112	102	8	29/5	12	
39	1.43E-04	2.72E-05	1.021	0.008	1.022	0.011	1.044	0.014	0.007	0.282	140	4	15/7	49	
40	1.11E-04	3.07E-05	1.011	0.005	1.009	0.005	1.021	0.006	-0.085	0.408	83	13	26/14	339	
41	1.19E-04	3.30E-05	1.01	0.003	1.013	0.008	1.024	0.008	0.056	0.373	146	3	16/8	237	
42	8.48E-05	3.07E-05	1.018	0.007	1.023	0.015	1.042	0.023	0.067	0.168	223	44	58/7	97	
43	1.15E-04	2.16E-05	1.01	0.003	1.009	0.004	1.019	0.005	-0.058	0.234	313	8	13/10	219	
44	9.37E-05	3.09E-05	1.013	0.009	1.05	0.038	1.069	0.044	0.494	0.428	311	1	26/11	41	
45	4.50E-05	1.21E-05	1.009	0.003	1.012	0.01	1.022	0.013	0.027	0.384	298	7	12/9	208	
46	4.46E-04	1.05E-05	1.02	0.011	1.089	0.017	1.119	0.016	0.617	0.211	352	2	43/8	83	

47	1.13E-04	3.61E-05	1.007	0.007	1.013	0.008	1.022	0.01	0.308	0.435	260	9	24/16	0
48	3.42E-04	4.07E-04	1.019	0.013	1.027	0.019	1.047	0.031	0.171	0.255	254	33	13/6	62

Table 3. Orientation of the magnetic ellipsoid and confidence angles of the samples at low temperature (LT) and the same samples at room temperature (RT selected) averaged for the selected sites and after bedding corrected to horizontal. LT/RT: Relationship between low temperature magnetic susceptibility and room temperature magnetic susceptibility. Average value of magnetic susceptibility (Km), standard magnetic lineation (L) foliation (F), corrected anisotropy degree (Pj) and shape parameter (T) of every site, with the corresponding standard deviation.

			kmax		conf. ang.	kint		conf. ang.	kmin		conf. ang.	LT/RT	average		average		average
	site	N	dec	inc		dec	inc		dec	inc			Km	stand. dev.	L	stand. dev.	F
RT selected	AG28	8	99	10	22/8	195	31	55/16	354	57	54/8		5.78E-05	2.92E-05	1.007	0.006	1.008
LT	AG28	8	91	2	19/12	185	66	28/17	1	24	28/12	1.40	8.08E-05	4.26E-05	1.005	0.004	1.007
RT selected	AG30	6	304	5	14/7	36	13	12/9	194	77	14/11		1.51E-04	2.34E-05	1.014	0.003	1.031
LT	AG30	6	303	3	14/5	33	14	17/8	200	76	17/6	1.97	2.97E-04	7.13E-05	1.014	0.003	1.027
RT selected	AN7	8	314	4	18/8	224	19	12/9	65	79	12/9		1.80E-04	2.69E-05	1.009	0.003	1.027
LT	AN7	8	320	4	28/12	229	11	28/12	71	78	12/8	2.33	4.19E-04	7.16E-05	1.007	0.002	1.027
RT selected	TT7	7	52	0	29/14	322	20	28/12	142	70	17/12		1.29E-04	1.85E-05	1.005	0.002	1.018
LT	TT7	7	300	5	52/13	30	2	52/13	139	84	19/13	1.67	2.15E-04	2.53E-05	1.004	0.002	1.014
RT selected	AG24	7	17	80	17/8	277	2	19/16	186	10	19/8		9.57E-05	3.98E-05	1.01	0.006	1.006
LT	AG24	7	287	15	31/6	188	31	82/24	39	55	82/20	1.80	1.72E-04	8.63E-05	1.007	0.002	1.007
LT(low LT/RT eliminated)	AG24	5	287	12	25/5	196	5	25/12	83	77	25/17	2.03	1.94E-04	8.76E-05	1.007	0.001	1.008
RT selected	AG36	7	264	5	3/3	99	84	6/3	354	5	5/3		5.27E-04	1.19E-04	1.077	0.013	1.039
LT	AG36	7	269	7	5/2	95	83	5/5	359	1	5/2	0.74	3.88E-04	6.40E-05	1.019	0.004	1.018
RT selected	AG26	7	87	61	25/7	273	29	23/10	181	3	15/8		8.91E-05	2.685-5	1.011	0.004	1.024
LT	AG26	7	98	14	22/5	318	72	19/15	191	11	19/11	1.38	1.23E-04	4.18E-05	1.006	0.003	1.007
RT selected	AG32	7	90	2	31/10	201	83	37/16	359	6	29/6		1.25E-04	2.94E-05	1.008	0.003	1.008
LT	AG32	7	90	3	10/7	352	56	66/6	179	34	66/9	2.01	2.51E-04	7.55E-05	1.007	0.005	1.006
RT selected	TT5	7	219	4	12/4	326	76	13/10	127	14	11/4		3.35E-04	3.27E-05	1.039	0.007	1.026
LT	TT5	7	226	0	10/4	316	38	49/10	135	52	49/4	0.89	2.97E-04	2.28E-05	1.009	0.002	1.007
RT selected	TT3	5	46	80	7/4	208	10	35/4	299	3	35/3		2.26E-04	2.36E-05	1.013	0.005	1.015
LT	TT3	5	177	4	34/12	268	3	33/16	31	85	20/9	1.00	2.27E-04	3.59E-05	1.006	0.003	1.013